Geomatics, Natural Hazards and Risk

ISSN: (Print) (Online) Journal homepage: https://www.tandfonline.com/loi/tgnh20

Estimation of changes in runoff and its sources in response to future climate change in a critical zone of the Karakoram mountainous region, Pakistan in the near and far future

Muhammad Adnan, Shiyin Liu, Muhammad Saifullah, Mudassar Iqbal, Qaisar Saddique, Waqas Ul Hussan & Yasir Latif

To cite this article: Muhammad Adnan, Shiyin Liu, Muhammad Saifullah, Mudassar Iqbal, Qaisar Saddique, Waqas Ul Hussan & Yasir Latif (2024) Estimation of changes in runoff and its sources in response to future climate change in a critical zone of the Karakoram mountainous region, Pakistan in the near and far future, Geomatics, Natural Hazards and Risk, 15:1, 2291330, DOI: 10.1080/19475705.2023.2291330

To link to this article: https://doi.org/10.1080/19475705.2023.2291330

GEOMATICS, NATURAL HAZARDS AND RISK
2024, VOL. 15, NO. 1, 2291330
https://doi.org/10.1080/19475705.2023.2291330

Estimation of changes in runoff and its sources in response to future climate change in a critical zone of the Karakoram mountainous region, Pakistan in the near and far future

Muhammad Adnan[a], Shiyin Liu[a,b], Muhammad Saifullah[c], Mudassar Iqbal[d], Qaisar Saddique[e], Waqas Ul Hussan[f] and Yasir Latif[g]

[a]Institute of International Rivers and Eco-security, Yunnan University, Kunming, Yunnan, China; [b]Yunnan International Joint Laboratory of China-Laos-Bangladesh-Myanmar Natural Resources Remote Sensing Monitoring, Kunming, Yunnan, China; [c]Department of Agricultural Engineering, Muhammad Nawaz Shareef University of Agriculture, Multan, Pakistan; [d]Centre of Excellence in Water Resources Engineering, University of Engineering and Technology, Lahore, Pakistan; [e]Member of the Leibniz Association, Postdam Institute for Climate Impact Research, Telegrafenberg, Germany; [f]Department of Irrigation and Drainage, University of Agriculture, DI Khan, Pakistan; [g]Institute of Computer Sciences, Czech Academy of Sciences, Prague, Czechia

ABSTRACT

The inconsistent pattern of precipitation, a shift in the seasonality of river flows, and the early onset of snow and glacier melt in recent decades across river basins of High Mountain Asia (HMA) has compelled us to further investigate future variations in sources of runoff under projected climate change scenarios. This will help in determining the timing and magnitude of runoff components and this will help in management of future water resources. The current study employed the University of British Columbia Watershed Model (UBC WM) to estimate the spatiotemporal variations in simulated runoff components (i.e. snowmelt, glacier melt, rainfall-runoff, and baseflow) and their relative contribution to total runoff of Gilgit River regarding the baseline period (1981–2010) in near (2021–2050) and far future (2071–2100) under low (SSP1), medium (SSP2) and high (SSP5) emission scenarios. A significant increase in the magnitude of mean annual temperature and precipitation is expected in the near future (2021–2050) than far future (2071–2100) under most SSPs. Moreover, high-altitude stations of the Gilgit River basin are expected to experience more warming in the near and far future than low altitudes under all SSPs. On average, regarding the baseline period, the simulated runoff is projected to increase in the near (27%, 30%, and 33%) and far future (30%, 53%, and 91%) under SSP1, SSP2, and SSP5, respectively. Moreover, an early onset of snow/glacier melting is predicted in the far future due

ARTICLE HISTORY
Received 17 August 2023
Accepted 30 November 2023

KEYWORDS
Gilgit River basin; general circulation model; shared socioeconomic pathways; UBC WM; climate change; runoff

CONTACT Shiyin Liu shiyin.liu@ynu.edu.cn

to an increase in summer air temperature and a decline in winter (DJF) precipitation. Besides, the rise in high altitude temperature is expected to cause the melting of snow/glaciers even above 6000 m elevation in the far future.

1. Introduction

The water coming from Hindu-Kush, Karakoram, and Himalayas (HKH) mountain ranges which are also known as Earth's third pole plays a vital role to fulfill the requirements of downstream inhabitants (Soncini et al. 2015) and also contributes a substantial amount of water to the streamflows of Indus River (Yu et al. 2013). Climate change has turned into the greatest challenge for the HKH region in the twenty first century (Dahri et al. 2021) and it has repercussions for water resources through increasing temperature, changing the timing of snowfall and glacier melt, fluctuating precipitation patterns, and ultimately changes in the seasonality of streamflows (Ougahi et al. 2022). Due to these noteworthy alterations in the hydro-meteorological regime, the HKH region and allied high-altitude Indus basin have been regarded as a 'hotspot' of climate change (Kraaijenbrink et al. 2017; Wijngaard et al. 2018; Krishnan et al. 2019; Lutz et al. 2019). The future projections also revealed an increase in the mean annual air temperature of the Upper Indus Basin (UIB) between 0.8 and 5.7 °C by the end of the twenty first century (Dahri et al. 2021) while another conducted by Lutz et al. (2019) predicted a temperature increase of 2.1 and 2.7 °C in a 1.5 and 2 °C warmer world, respectively, in the HKH region. Besides, it has been predicted that under the 1.5 °C scenario of global warming; the warming in the northwest Himalaya and Karakoram is projected to be 0.7 °C higher than global warming (Krishnan et al. 2019). Moreover, an increase in streamflows of UIB is estimated to be 34 and 43% in a 1.5 and 2 °C warmer world, respectively (Ul Hasson et al. 2019) while another study (i.e. Su et al. 2022) disclosed an increase in the streamflows of the Indus River in the first half of the twenty first century due to enhanced glacier melting.

The current study will be conducted on the main sub-catchment of UIB (i.e. Gilgit River basin) located in the north-western Karakorum. The sub-catchment Gilgit receives combined streamflows of Gilgit and Hunza Rivers at Alam Bridge gauging station just before joining the Indus River (Adnan et al. 2022). The study area is highly vulnerable to climate change and the development of several glacial lakes has been witnessed in recent years which has caused Glacial Lake Outburst Floods (GLOFs) events in the basin such as Shisper glacial lake (Saifullah et al. 2020; Gao et al. 2021), which bursts every year since its development in 2019. The previous studies have projected that the climate change impacts on the hydrological regime of this region will continue till the end of the twenty first century (Wijngaard et al. 2017; Krishnan et al. 2019; Dahri et al. 2021). In this perspective, several studies projected future streamflows of the Hunza River basin such as (Garee et al. 2017; Ali et al. 2018; Hayat et al. 2019; Dolk et al. 2020; Fatima et al. 2020; Nazeer et al. 2022) while few studies attempted to project future streamflows of Gilgit River basin at

Gilgit station such as (Adnan et al. 2017; Latif et al. 2020) under Representative Concentration Pathways (RCPs) scenarios. A study conducted by Garee et al. (2017) predicted a 5 to 10% increase in streamflows of the Hunza River as a result of a 31% increase in precipitation and a 1.39 to 6.58 °C rise in temperature by the end of the twenty first century. Another study performed by Ali et al. (2018) estimated a 22 to 88% increase in streamflows of the Hunza River under RCP4.5 towards the end of the twenty first century. Similarly, Hayat et al. (2019) predicted a 14 to 90% increase in the mean annual discharge of Hunza River under all RCPs during the mid to late-twenty first century. Similarly, Fatima et al. (2020) also estimated a substantial increase in streamflows of the Hunza River under all RCPs throughout the twenty first century. Likewise, under the scenario of no glacier shrinkage, it has been projected a 54 to 125% increase in future streamflows of Hunza River by Dolk et al. (2020) from 2046 to 2075. However, Nazeer et al. (2022) projected a 23 to 126% increase in streamflows of the Hunza River due to a 12 to 32% increase in precipitation and a 1.1 to 8.6 °C increase in mean annual temperature throughout the twenty-first century. Besides, a study performed by Adnan et al. (2017) estimated a 67% increase in mean annual discharge of the Gilgit River due to an increase of 3 °C under RCP4.5 by the end of the twenty first century. Likewise, another study conducted by Latif et al. (2020) estimated a 5.6 to 19.8% increase in summer flows of the Gilgit River due to a rise in mean annual temperature between 0.7 and 2.6 °C during 2039–2070.

The past studies conducted on sub-catchments of the UIB projected the streamflows under climate change scenarios but did not estimate the changes and trends in runoff components under the latest climate change scenarios. Besides, the hydrological models used in the previous studies (i.e. Tahir et al. 2011; Adnan et al. 2017; Garee et al. 2017; Hayat et al. 2019; Latif et al. 2020) such as the Snowmelt Runoff Model (SRM) and Soil and Water Assessment Tool (SWAT) were lack of glacier modules and they also failed to provide credible information about baseflow which is an important component of winter streamflows. Moreover, the previous research did not determine the future relative contribution of runoff components to the streamflows of the Gilgit River at Alam Bridge under Shared Socioeconomic Pathways (SSPs) of Coupled Model Intercomparison Project Phase 6 (CMIP6). However, our previous study (i.e. Adnan et al. 2022) determined the spatiotemporal variations of runoff components to the streamflows of Gilgit River while the current study is an extension of our previous study, and in this study, we will estimate the spatiotemporal variations of runoff components and their relative contribution to the future streamflows under SSPs. The main objectives of the current study include: (1) to estimate the future change in the magnitude of climatic variables i.e. temperature and precipitation of Gilgit River basin during near (2021–2050) and far future (2071–2100) under low (SSP1–2.6), medium (SSP2–4.5) and high (SSP5–8.5) emission scenarios, (2) to estimate the change in future streamflows of Gilgit River at annual and seasonal time scales with respect to baseline period in near and far future periods, (3) to predict the spatiotemporal variations in relative contributions of runoff components to the streamflows of the Gilgit River during near and far future periods under SSPs.

2. Materials and methods

2.1. Study area

The area covered by the Indus River basin upstream of Tarbela Dam is known as UIB and more than 60% of streamflows of the Indus River at Tarbela are contributed in the form of snow and glacier melting (Hasson et al. 2017; Latif et al. 2020). There are mainly 7 major sub-basins of the UIB named Gilgit, Astore, Hunza, Shingo, Shyok, Shigar, and Zanskar. The Gilgit River basin at Alam Bridge is the main sub-catchment of the UIB located in the western part of the Karakoram mountain range (Figure 1). The boundary of the Gilgit River basin ranged between latitude 35.71°–37.09°N and longitude 72.51°–75.78°E. The mean elevation of the study area is 4230 m. The study area encompasses the Gilgit, Hunza, Nagar, and Ghizer localities of the Gilgit–Baltistan Province. There are steep mountains, valleys, and some highest peaks of the Karakoram mountain range. The basin elevation ranges from 1178 to 7850 m and a major portion of the study area (i.e. 88%) falls between elevations 4000–5500 m (Hussain et al. 2019) whereas about 46% part of the study area exists between elevations 4000–5000 m (Table 1) (Adnan et al. 2022).

The catchment area of the Gilgit River basin at Alam Bridge station is 27,272 km^2 and out of which about 20% area (i.e. 5456 km^2) of the basin is covered by glaciers. Moreover, the study area comprised 8 meteorological stations installed from low to high elevations such as Hunza, Naltar, Khunjerab, Ziarat, Gilgit, Gupis, Yasin, and Ushkore, while the number of stream gauging stations is 3 such as Gilgit, Dainyore, and Alam Bridge as shown in Figure 1. The Gilgit River flows from northwest to southeast whereas the Hunza River flows from north to south and both the rivers join together at Alam Bridge which is located just

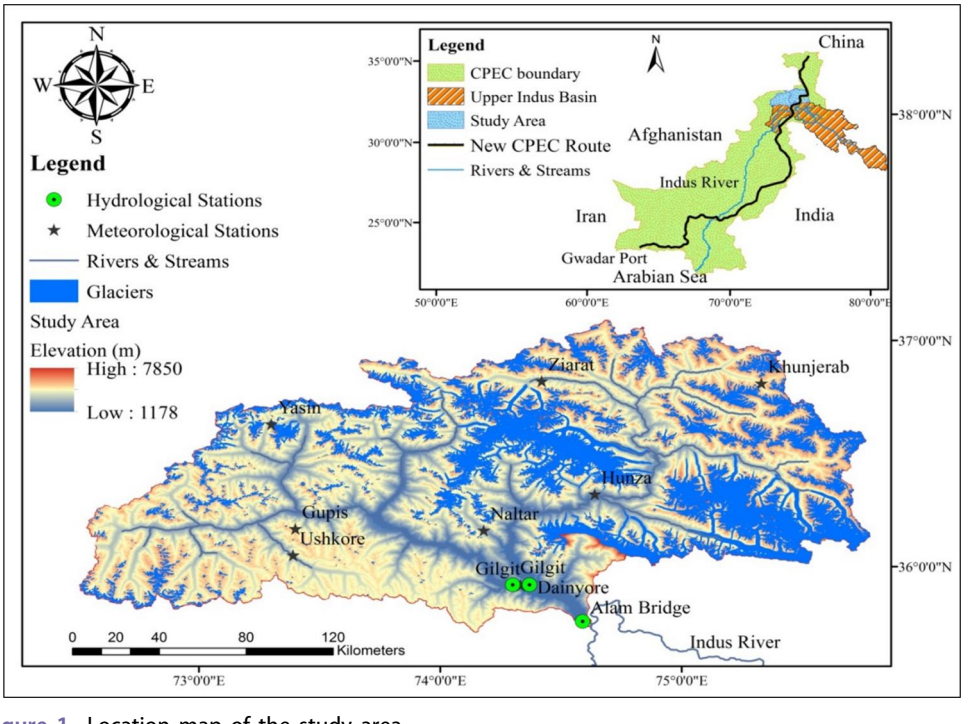

Figure 1. Location map of the study area.

Table 1. Terrain features of the study area.

Serial No.	Elevation bands (m)	Mean elevation (m)	Band area (km^2)	Glacier area (km^2)	% of Glacier area
1	1178–2012	1595	494.03	0	0
2	2012–2846	2429	1731.85	14.7	0.27
3	2846–3680	3263	4177.78	244.3	4.48
4	3680–4514	4097	9232.59	873.2	16.01
5	4514–5348	4931	9024.24	2496.4	45.78
6	5348–6182	5765	2221.63	1495.8	27.43
7	6182–7016	6599	311.55	287.2	5.27
8	7016–7850	7433	43.03	41.3	0.76
Total			27,236	5452.9	100

downstream of Gilgit town whereas the Gilgit River joins the Indus River at Jaglot (Partab Bridge). The mean annual discharge of Gilgit River (i.e. from 1981 to 2015) at Alam Bridge was 617 m^3/s. Furthermore, the maximum and minimum discharge values of the Gilgit River at Alam Bridge were 4834 m^3/s and 66.1 m^3/s, respectively, during the specified period. The major part of the Gilgit River flows i.e. 26% is contributed to the Indus River in July while 24% in August (Adnan et al. 2022). The Gilgit River basin falls in the category of cold desert climate system and it receives summer precipitation due to monsoon season while winter/spring precipitation due to westerlies system. The major portion of annual precipitation occurs in the winter and spring seasons in the form of snow (Hewitt 2011; Ul Hussan et al. 2020). The monthly average summer temperature in the study area varies from 5.6 to 26.5 °C in July while the monthly average winter temperature of the study area varies from 3.8 to −16.7 °C in January (Adnan et al. 2022). The major land-cover classes of the study area include soil/rock (48.8%), snow/glaciers (31.4%), alpine grasses and shrubs (17.4%), and agricultural land (1.34%) whereas the minor classes are dense & sparse coniferous and mixed forests (0.82%) and water bodies (0.25%) as shown in Figure 2.

2.2. Datasets

The datasets used in this study are listed in Table 2. A comprehensive description of these datasets is given below:

2.2.1. Topographic data

The Advanced Spaceborne Thermal Emission and Reflection Radiometer (ASTER), Global Digital Elevation Model (GDEM) version-3 data of 30 m resolution was acquired from the website: https://lpdaac usgs.gov/tools/data-pool/to delineate catchment boundary of the Gilgit River basin in ArcGIS 10.2. The GDEM of the study area clipped from the main tile has an elevation ranging from 1178 to 7850 m.

The glacier data of Southwest Asia was downloaded from the Randolph Glacier Inventory 6.0 repository and then the glacier data of the Gilgit basin was clipped from the source map. The glaciated area of the Gilgit River basin was estimated to be 20% (i.e. 5456 km^2) and out of the total glaciated area nearly 45.78% (or 2496 km^2) was found between elevations ranging from 4514 to 5328 m whereas approximately 27.4% was observed between elevations 5348 and 6182 m (Table 1). Moreover, Pakistan's lands cover data of (30 × 30 m) grid resolution was managed from the International Centre for Integrated Mountain Development (ICIMOD) data archive (Table 2).

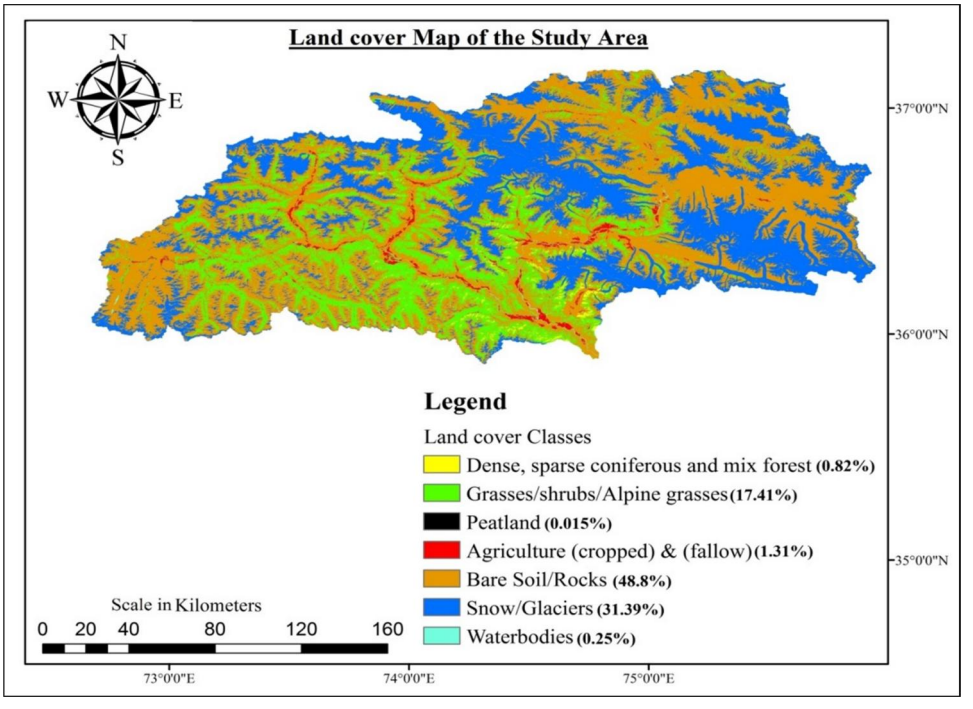

Figure 2. Land cover map of the study area.

Table 2. List of datasets used in the current study.

Data Type	Description	Resolution	Period	Source
Digital Elevation Model	ASTER GDEM ver.3	30 m	–	https://lpdaac.usgs.gov/tools/data-pool/
Land cover	ICIMOD	30 m	2010	https://doi.org/10.26066/rds.28630
Glacier	Randolph Glacier Inventory 6.0	Vector data	2017	https://doi.org/10.7265/N5-RGI-60
Meteorological Data	T_{max}, T_{min}, T_{avg}, Precipitation,	Daily	1981–2015	Pakistan Meteorological Department (PMD) Surface Water Hydrology Project of Water and Power Development Authority, Pakistan (SWHP-WAPDA)
ERA5 Data	2m T_{max}, T_{min} and T_{avg}, Total Precipitation	Hourly ($0.25^{\circ} \times 0.25^{\circ}$)	1981–2020	https://cds.climate.copernicus.eu/cdsapp#!/dataset/reanalysis-era5-single-levels?tab=overview
CMIP6 Global Circulation Models (GCMs)	T_{max}, T_{min} and T_{avg}, Pr	Daily	1981–2100	Lawrence Livermore National Laboratory, Department of Energy https://esgf-node.llnl.gov/search/cmip6/
Discharge Data	Gilgit River at Alam Bridge	Daily	1981–2015	Surface Water Hydrology Project of Water and Power Development Authority, Pakistan (SWHP-WAPDA)

Note: T_{max}, T_{min} and T_{avg} refer to maximum, minimum, and average temperature respectively, and P_r refers to precipitation.

Table 3. List of hydro-meteorological stations used in the study.

Station	Latitude (DD)	Longitude (DD)	Elevation (m)	Data used	Source of data
Meteorological stations					
Gilgit	35.917	74.333	1460	1981–2015	PMD
Gupis	36.167	73.400	2156	1981–2015	PMD
Ziarat	36.830	74.430	3688	1995–2012	SWHP-WAPDA
Khunjerab	36.850	75.400	4440	1995–2012	SWHP-WAPDA
Streamflows gauging station					
Alam Bridge	35.758	74.59	1280	1981–2015	SWHP-WAPDA

Note: 'DD' denotes degree decimals.

2.2.2. Observed hydro-meteorological data

The daily observed streamflows and climatic data were gotten from the Pakistan Meteorological Department (PMD) and Surface Water Hydrology Project of Water and Power Development Authority, Pakistan (SWHP-WAPDA) from 1981 to 2015 (Table 3). The daily climatic data of 4 observatory stations (i.e. Gilgit, Gupis, Ziarat, and Khunjerab) include average temperature, minimum-maximum temperature, and precipitation whereas the discharges data of Gilgit River at Alam Bridge gauging station was used for this study (Table 3). The daily observed climatic data was available from 1981 to 2015 for Gilgit and Gupis while it was available from 1995 to 2012 for Ziarat and Khunjerab stations. The daily climatic data from 1981 to 2020 was prepared for above mentioned 4 climatic stations with the help of observed and reanalysis data such as the European Environment Agency (ERA5) to force the hydrological model.

2.2.3. Reanalysis data

The European Environment Agency (ERA5) hourly data of ($0.25^{\circ} \times 25^{\circ}$) resolution for mean, minimum, and maximum temperature and precipitation was downloaded from the 'Copernicus Climate Date Store' from 1981 to 2020 to complete and prepare the daily observed meteorological data (Table 2). Time series data of temperature and precipitation for each climatic station was extracted from ERA5 raster data and then this data was bias-corrected against observed climatic data by empirical relations presented by Sperna Weiland et al. (2010) and Cheng and Steenburgh (2007), respectively. The detail of these empirical relations is given in our previous study (i.e. Adnan et al. 2022). The daily ERA5 bias-corrected data of precipitation, the minimum, and maximum temperature was used to fill in the missing data of Gilgit and Gupis from 2016 to 2020 while in the case of Ziarat and Khunjerab; the missing data records were filled from 1981 to 1994 and then from 2013 to 2020 and thus we prepared climatic data of 4 stations from 1981 to 2020.

2.2.4. General circulation model (GCM) data

CMIP6 GCM data was downloaded from the Lawrence Livermore National Laboratory data archive. Three GCMs, i.e. (ACCESS-ESM1-5, BCC-CSM2-MR, and MRI-ESM2-0) were selected based on comparison with the observed meteorological data. The selected GCMs are listed in Table 4. The GCM data of precipitation and the minimum, maximum, and average temperature were downloaded for the historic (1950–2014) and projected (2015–2100) periods under low (SSP1–2.6), medium

Table 4. List of selected GCMs for climate change study.

Model	Name	Country	Spatial Resolution (Latitude × Longitude)
ACCESS-ESM1-5	The Australian Community Climate and Earth System Simulator Earth System Model	Australia	(1.25° ×1.875°)
BCC-CSM2-MR	Beijing Climate Center Climate System Model	China	(1.1215° ×1.125°)
MRI-ESM2-0	The Meteorological Research Institute Earth System Model Version 2.0	Japan	(1.1215° ×1.125°)

(SSP2–4.5) and high (SSP5–8.5) emission scenarios. Time series data of four meteorological stations (i.e. Gilgit, Gupis, Ziarat, and Khunjerab) was extracted from three GCMs separately and then ensemble mean data of these GCMs was prepared for the historic (1981–2014) and projected (2015–2100) period under low, medium and high SSPs.

2.2.5. Downscaling of GCM data

The ensemble mean GCMs data were bias-corrected by using Generator for Point Climate Change (GPCC) model before its comparison with the observed meteorological data. GPCC is a statistical climate downscaling model which was developed by Zhang (2005). The model is based on the stochastic weather generator CLIGEN and it downscales monthly projections of GCMs in a grid box to daily weather series at a point scale or station. It downscales precipitation, maximum and minimum temperatures. Observed T_{max}, T_{min}, T_{avg}, and precipitation data of Gilgit, Gupis, Ziarat, and Khunjerab stations were compared with historic GCMs ensemble mean data for the period 1981–2012, and found satisfactory results with R^2 values > 0.80 and RMSE $<$ 5.0 in most of the cases except precipitation (see Appendix Figures A1–A4). However, the historical GCM precipitation data displayed large uncertainties in terms of magnitude and spatial distribution with reference to observed data (see Appendix Figure A4). Even bias-corrected precipitation of GCM failed to capture extreme precipitation events and spatial distribution and displayed low values of $R^2 < 0.20$ and RMSE $=$ 14–34.

2.3. Hydrological modeling

The current study will use UBC WM to project future streamflows and future relative contribution of runoff components to the total runoff of the Gilgit River under SSPs at spatiotemporal scales. A detailed description of UBC WM is given below:

2.3.1. UBC watershed model

Quick and Pipes (1972; 1977) developed the University of British Columbia Watershed Model (UBC WM) for streamflows forecasting of the Fraser River system in British Columbia. The concept of the area-elevation band was introduced in UBC WM for streamflow forecasting in the mountainous catchment. The input data used in the hydrological model include hourly or daily minimum and maximum temperature, precipitation, and streamflows and the output file includes simulated runoff, snowmelt runoff, glacier melt runoff, rainfall-runoff, baseflow, and snowpack accumulation/depletion. For the process flow diagram of the hydrological model (see

Appendix Figure A5). The simulated runoff in the model is further subdivided into a fast, medium, slow, and very slow flow based on soil moisture and groundwater characteristics. In the case of a mountainous catchment, the amount of snowmelt and rain input to each elevation band is further separated based on priority to satisfy the soil moisture deficit which constantly diminished because of change in the demand of evaporation. The model uses a simple energy balance approach with temperature data as input for the calculation of snowmelt. In UBC WM, the spatial distribution of precipitation and temperature is controlled by the area-elevation band theory. In hydrological model settings, the catchment is sub-divided into 4 to 12 elevation bands (ideally 8 elevation bands) and then the point measurement of temperature and precipitation is extrapolated to the mid-elevation of each band of the catchment based on lapse rates by the UBC WM. Besides, temperature lapse is used to control the snowmelt rate and the precipitation distribution at different elevations of the catchment in UBC WM, and the form of precipitation (i.e. rain or snow) is also decided in the model based on temperature and elevation inputs. The UBC WM uses an energy method of melting snow and glaciers. In the simple energy method temperature data is used for the calculation of melt rates whereas in the complex version of the energy method, detailed information related to solar radiation, albedo, and wind speed is required which is mostly not available in high altitude basins which may produce uncertainty in results. Secondly, several parameters/factors dealing with this melting process of snowpack and glacier melt are fixed (default) and are advised by the developer of UBC WM not to change them without practical knowledge of the study area. These parameters/factors are related to snowpack, glacier, short and longwave solar radiation, wind speed, albedo, cloud cover, condensation and convection, etc. So, these default parameters may also produce uncertainty in results to some extent. Besides, a few other factors such as glaciated area and fraction of glaciated area with south orientation are calculated for each elevation band. The UBC WM calculates snowmelt, glacier melt, and rainfall runoff in each elevation band based on parameters/factors, variables, and lapse rates. Among these, the temperature lapse rate is very important for determining the snowmelt rates at various elevations because it largely impacts precipitation distribution in each elevation band. The precipitation falls as snow accumulates as snowpack in each elevation band and then depleted based on the calculated melt rate. The process of snow accumulation and depletion occurs distinctly in each elevation band. The snow/glacier melt and rainfall runoff produced in each elevation band of the watershed is controlled by the soil moisture model which further sub-divides these runoffs into the different components of watershed runoff response such as fast (surface runoff), medium (interflow), slow (superficial groundwater) and very slow (deep groundwater) components (see Appendix Figure A5). Besides, this watershed model is capable of controlling snow cover area and glacier extent.

2.3.2. Hydrological model's settings

The minimum requirement of meteorological stations input for forcing the UBC WM is 1 while the maximum limit is 5. The meteorological stations beyond 5 are beyond the limit of the UBC WM. So, the current study selected four

meteorological stations having long-term observed data and installed at different elevations ranging from 1460 to 4440 m in the Gilgit River Basin to force the hydrological model. These meteorological stations are located at low, mid, and high altitudes and thus represent the meteorological characteristics of the whole Gilgit River basin. However, the spatial distributions of climatic variables (i.e. temperature and precipitation) will be controlled by the UBC WM through area-elevation band theory where the observed point data is extrapolated to the mid-elevation of each band of the catchment based on lapse rates. In the UBC WM model's setting, the watershed can be divided up to 12 elevation bands while it is ideal to divide the basin into 4–8 elevation bands (Quick and Pipes 1977; Loukas and Vasiliades 2014). In the current study, the watershed was divided into four aspect classes (i.e. north, south, east, and west) and 8 elevation bands. The information related to the north/south orientation of the hillside and fraction of the south facing of the hillside was determined for each elevation band and inputted to the watershed file (.WAT) of UBC WM. Besides, the parameters related to topography and land cover were also calculated for each elevation band such as impermeable area, mean elevation, glacier cover area, band area, canopy, and forest density, and then inputted into the (.WAT file) of the UBC WM.

2.3.3. Calibration and validation analysis

The calibration (1981–2000) and validation (2001–2015) of the UBC WM were performed in our previous study on the Gilgit River basin (i.e. Adnan et al. 2022) as displayed in Figure 3(a,b). The calibrated parameters are listed in Table 5. During the calibration process, few parameters were found more sensitive to streamflows such as

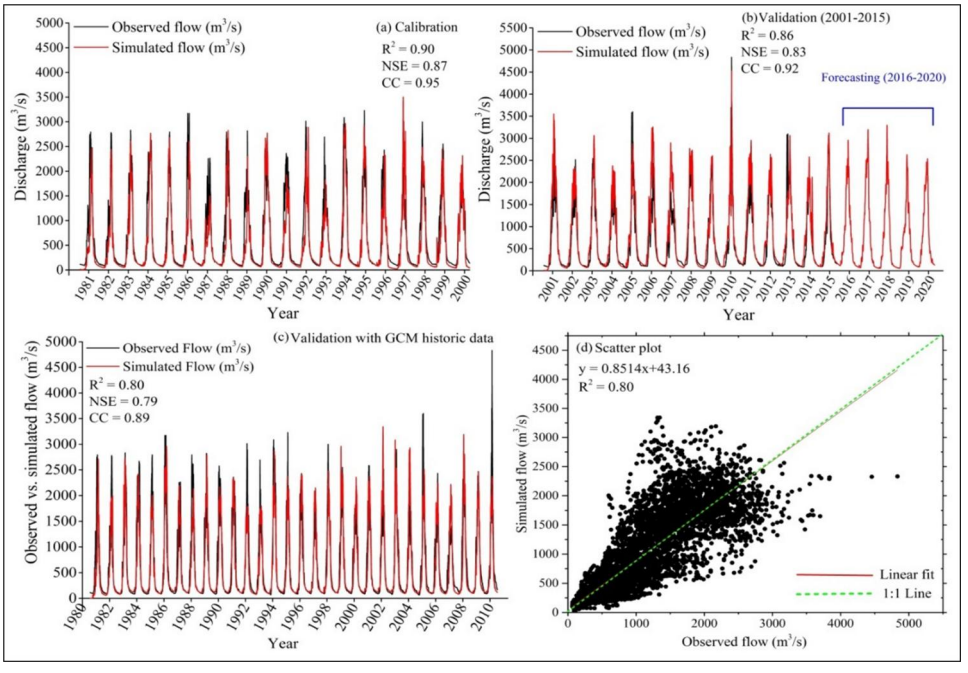

Figure 3. (a, b) Calibration and validation of UBC WM with observed data, (c, d) validation of UBC WM with GCM historic data before prediction of future streamflows.

Table 5. List of parameters calibrated in UBC WM.

Parameters	Description	Value
Precipitation		
P0SREP	AES adjustment factor for snowfall data	0.822
P0RREP	AES adjustment factor for rainfall data	0.768
P0GRADL	Precipitation gradient factor for elevations below E0LMID, %	10
P0GRADM	Precipitation gradient factor for elevations below E0LHI, %	19
P0GRADU	Precipitation gradient factor for elevations above E0LHI, %	15
E0LMID	Elevation above which precipitation gradient P0GRADM applies. Set at approx. 1/2 barrier height, (m)	3336
E0LHI	Elevation above which the precipitation gradient P0GRADU applies. Set at approx. 2/3 barrier height,(m)	4450
Water		
P0PERC	Groundwater percolation. (Maximum capacity of sub-surface storage. Excess runoff goes to interflow.) Units of mm	23.97
P0DZSH	Deep zone share (lower fraction) of groundwater	0.81
P0AGEN	Impermeable area modification factor. It is compared with how much moisture has satisfied the soil demands and used in an exponential decay function. Units of mm	100
C0IMPA	Fraction of impermeable area for the band	0.075
Routing		
V0FLAS	Flash flood threshold, mm (If runoff greater than V0FLAS, FLASH SHARE is initiated), mm	40
P0FRTK	Rainfall fast runoff time constant (days)	1.93
P0FSTK	Snowmelt fast runoff time constant (days)	1.48
P0GLTK	Glacial melt fast runoff time constant (days)	1.94
P0IRTK	Rainfall interflow component time constant (days)	3.64
P0ISTK	Snow melt interflow component time constant (days)	2.91
P0UGTK	Upper groundwater runoff time constant (days)	48.76
P0DZTK	Deep zone share (lower groundwater) time constant	218.09
Other Sensitive Parameters		
LAPSER	Index for Temperature Lapse Rate (=1 for algorithm; 2= Climate stations)	1
IGRADP	Index for Precipitation Lapse Rate (=1 for algorithm; 2= Interpolation)	1
AOEDDF	Potential evapotranspiration factor in mm/day	1.2
P0ALBMAX	Albedo of fresh snow	0.95
P0ALBMIN	An albedo of very aged snowpack	0.40
LAGS	Lag in snowmelt distribution (0 or 1 time step)	1
LAGR	Lag in rainfall distribution (0 or 1 time step)	0

those related to precipitation (P0SREP, P0RREP, P0GRADL, and P0GRADM), elevation (E0LMID, E0LHI), water (C0IMPA, P0DZSH, P0AGEN, P0PERC), and routing such as P0UGTK, P0DZTK and V0FLAS. Before the projection of future streamflows, the UBC WM was validated with historic data of GCM and got excellent results as shown in Figure 3(c,d).

2.3.4. Future scenarios for runoff projections

The daily ensemble mean data of future projected minimum/maximum temperature and precipitation were input to the UBC WM for simulation of future streamflows of Gilgit River under different SSPs scenarios. The bias-corrected ensemble mean data of GCMs was divided into 3 periods such as baseline (1981–2010), near future (2021–2050), and far future (2071–2100), and projections were made under low (SSP1–2.6), medium (SSP2–4.5) and high (SSP5–8.5) emission scenarios.

2.3.5. Trend analysis

The current study employed the Mann-Kendall test (MK) (Mann 1945; Kendall 1975) to determine the monotonic upward or downward trend in the time series data of

climatic variables such as (T_{max}, T_{min}, T_{avg} and Pr) for the historic (1981–2010), near (2021–2050) and far future (2071–2100) periods under SSP2.6, SSP4.5 and SSP8.5. The MK test is non-parametric so it is less affected by outliers (Lanzante 1996). The MK test does not need data to be normally distributed and is less sensitive to abrupt breaks (Jaagus 2006).

The test statistics 'S' of the MK test is normally used for data whose sample size i.e. $n < 10$ as given below:

$$S = \sum_{k=1}^{n-1} \sum_{j=k=1}^{n} sgn(x_j - x_k) \tag{1}$$

where;

$$sgn\ (x_j - x_k) = \begin{cases} +1; & if\ (x_j - x_k) > 0 \\ 0; & if (x_j - x_k) = 0 \\ -1; & if (x_j - x_k) < 0 \end{cases} \tag{2}$$

where 'n' denotes the number of data points and x_j and x_k represents data values in time series j and k and (j > k). While $sgn\ (x_j - x_k)$ denotes sign function.

In another case, if the sample size is $n > 10$ then normal approximation such as standard normal test statistic (Z_s) is used and before that variance *VAR (S)* is calculated as given below in Equation (3).

$$VAR\ (S)\ = \frac{1}{18}\left[n(n-1)(2n+1) - \sum_{p=1}^{g} t_p(t_p-1)(2t_p+5)\right] \tag{3}$$

In the above Equation (3), $'n'$ denotes data points, $'g'$ denotes the number of equal trend values or tied groups whereas t_p describes the number of values in the P^{th} group.

Finally, in the MK test, Z_s is calculated by using the following Equation (4);

$$Z_s = \begin{cases} \dfrac{S-1}{\sqrt{VAR\ (S)}}; & S > 0 \\ 0; & S = 0 \\ \dfrac{S+1}{\sqrt{VAR\ (S)}} & S > 0 \end{cases} \tag{4}$$

The value of Z_s decides whether the trend in the time series is increasing or decreasing at the specific significance level (α). If the value of Z_s is positive then it means the trend is increasing and vice versa. Besides, the slope or magnitude of the trend was determined through Sen's slope test (Sen 1968).

2.3.6. Criteria for performance evaluation of hydro-meteorological data

The evaluation of comparisons between observed versus simulated streamflows of UBC WM and observed temperature and precipitation versus GCM historic data were performed through statistical relation of coefficient of determination (R^2), root mean square error (RMSE), and Nash–Sutcliffe efficiency (NSE) (Nash and Sutcliffe 1970). The empirical formulas of these statistical relations are represented by Equations (5)–(7);

$$R^2 = \frac{\left(\sum \left(Q_{obs} - \overline{Q}_{obs}\right)\left(Q_{sim} - \overline{Q}_{sim}\right)\right)^2}{\sum \left(Q_{obs} - \overline{Q}_{obs}\right)^2 \sum \left(Q_{sim} - \overline{Q}_{sim}\right)^2} \tag{5}$$

$$RMSE = \sqrt{\frac{\sum_{i=1}^{N}(Q_{obs} - Q_{sim})^2}{N}} \tag{6}$$

$$NSE = 1 - \frac{\sum \left(Q_{sim} - Q_{obs}\right)^2}{\sum \left(Q_{obs} - \overline{Q}_{obs}\right)^2} \tag{7}$$

where, Q_{sim} and Q_{obs} signify simulated and observed discharges, respectively whereas $\overline{Q}_{obs}$ and $\overline{Q}_{sim}$ denote mean observed and simulated discharges, respectively.

3. Results

3.1. Projected change in the magnitude of future climatic variables per period under different SSPs

The linear trend analysis unveiled an increasing trend in future projected maximum, minimum, and mean annual temperature magnitudes of the Gilgit River basin in the near (2021–2050) and far future (2071–2100) under all SSPs except SSP1 in the far future where it displayed a decreasing trend at all meteorological stations (see Appendix Figures A6–A8). On average, the magnitude of maximum temperature is predicted to increase with a change rate of 0.85, 1.10, and 1.84 °C per period in the near future and −0.31, 1.93, and 2.31 °C per period in the far future under SSP1, SSP2, and SSP5, respectively. Similarly, on average, the minimum temperature also displayed an increasing trend with a change rate of 0.94, 1.16, and 1.70 °C per period in the near future whereas −0.30, 0.74, and 2.05 °C per period in the far future under SSP1, SSP2 and SSP5, respectively. Likewise, the magnitude of mean annual temperature is also projected to increase with an average change rate of 0.87, 1.09, and 1.70 °C per period in the near future whereas −0.33, 0.77, and 2.10 °C per period in the far future under SSP1, SSP2, and SSP5, respectively. Overall, it has been estimated more an increase in the magnitudes of maximum, minimum, and average temperature in the near future than far future under SSP1 and SSP2 while under SSP5, the increase in temperature magnitude is estimated more in the far future than near future. Besides, the future projected maximum, minimum, and average temperature

displayed an increasing trend with greater change in magnitudes at high altitude stations than low altitude stations in the near and far future under all SSPs.

In the same way, the trend analysis indicated an increasing trend in the magnitude of annual precipitation of the Gilgit River basin at the majority of stations in the near and far future under all SSPs (see Appendix Figure A9). On average, during the baseline period, it exhibited a decreasing trend at a rate of −10.5 mm per period whereas it exhibited an increasing trend in the magnitude of annual precipitation at a rate of 14.8, 2.14, and 9.30 mm per period in the near future while 6.98, −0.38, and 4.57 mm per period in the far future under SSP1, SSP2, and SSP5, respectively. Overall, it is estimated more increase in the magnitude of annual precipitation in the near future than far future under all SSPs.

Moreover, on average, with reference to the baseline period, the mean annual precipitation of the Gilgit River basin is projected to increase by 6.4%, 5.85%, and 8.0% per period in the near future whereas 8.45%, 6.2%, and 12.9% per period in the far future under SSP1, SSP2, and SSP5, respectively (see Appendix Figure A10). Overall, the mean annual precipitation will gradually increase from low to high emission scenarios with reference to baseline periods in the near and far future under SSP1 and SSP5. However, there has been witnessed a drop in mean annual precipitation in the medium emission scenario (SSP2) as compared to SSP1 and SSP5 during both the near and far future.

3.2. Projected change in annual simulated runoff of Gilgit River basin under different SSPs

The modeling outcomes of UBC WM unveiled a substantial impact of projected climate change on the simulated runoff of Gilgit River in the near (2021–2050) and far future (2071–2100) with reference to the baseline period (1981–2010) under all SSPs as shown in Figure 4(a,b). Compared to precipitation, the rise in future projected temperature was found mainly responsible for increasing the simulating runoff of the Gilgit River basin by escalating melting rates of snow and glaciers under all SSPs. In the near future, it is predicted that the future simulated runoff in the Gilgit River basin will increase by 27%, 30%, and 33% per period with respect to the baseline period under SSP1, SSP2, and SSP5, respectively as shown in Figure 4(a).

Similarly, in the far future, the simulated runoff of Gilgit River is expected to increase by 30%, 53%, and 91% per period with respect to the baseline period under SSP1, SSP2, and SSP5, respectively.

3.3. Projected change in seasonal simulated runoff of Gilgit River basin under different SSPs

The predicted change in seasonal simulated runoff of the Gilgit River basin in the near (2021–2050) and far future (2070–2100) with respect to the baseline period (1981–2010) under different SSPs is displayed in Figure 5(a,b). Overall, the maximum increase in the simulated runoff is projected in summer (JJA) followed by spring (MAM), and autumn (SON) seasons from low (SSP1) to high (SSP5) emission

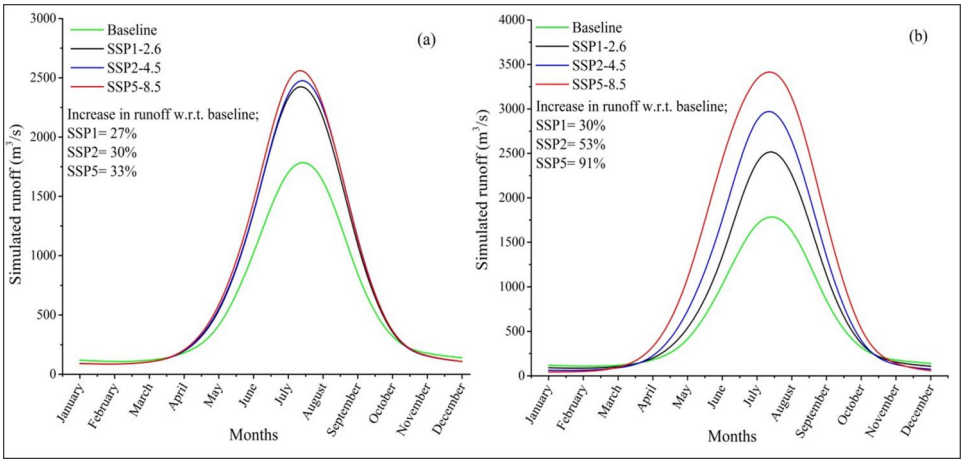

Figure 4. Projected change in annual simulated runoff of Gilgit River basin with respect to the baseline period (1981–2010), in (a) near future (2021–2050) and (b) far future (2071–2100) under different SSPs.

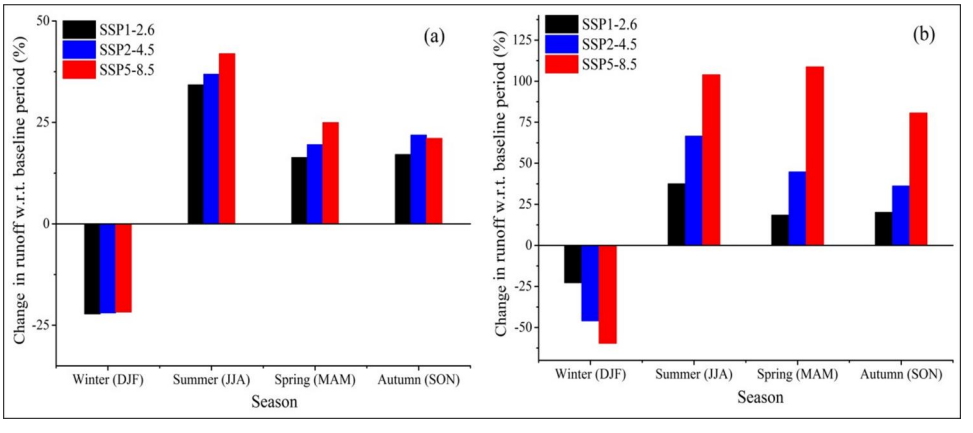

Figure 5. Projected change in seasonal simulated runoff of the Gilgit River basin with respect to the baseline period (1981–2010), in (a) near future (2021–2050) and (b) far future (2071–2100) under different SSPs.

scenarios, while the simulated runoff displayed a decreasing trend in winter (DJF) in the near and far future under all SSPs. In the near future, the simulated runoff in summer (JJA) is expected to increase by 34, 37, and 42% under SSP1, SSP2, and SSP5, respectively. However, in spring (MAM) and autumn (SON) seasons, the simulated runoff is projected to increase by (16, 20 and 25%) and (17, 22 and 21%) under SSP1, SSP2, and SSP5, respectively (Figure 5(a)).

Similarly, the simulated runoff of summer (JJA) is expected to increase by 37, 66, and 104% under SSP1, SSP2, and SSP5, respectively in the far future. However, under SSP5, it has been estimated more increase in simulated runoff of spring (MAM) than in autumn (SON) and summer (JJA) because of a substantial rise in spring (MAM) temperature (Figure 5(b)).

3.4. Projected change in simulated runoff from different altitudes of the Gilgit River basin under different SSPs

The projected change in the simulated runoff from different altitudes of the Gilgit River basin in the near (2021–2050) and far future (2071–2100) with respect to the baseline period (1981–2010) under different SSPs is displayed in Figure 6(a,b). Based on glacier cover area in the respective elevation bands; the maximum runoff generation is estimated from the fifth elevation band (4514–5348) followed by the sixth (5348–6182), fourth (3680–4514), and third (2846–3680) in the near and far future under all SSPs.

Moreover, it has been predicted a small contribution of simulated runoff i.e. <1 cumec from the first (1178–2012), second (2012–2846), and eighth (7016–7850) elevation bands in the near and far future under all SSPs. Besides, it has been expected that in the far future, the continuous increase in air temperature will cause the melting of snow/glaciers at elevations above 6000 m under SSP5 (Figure 6(b)).

3.5. Relative contribution of future projected simulated runoff components from different altitudes

The relative contribution of future projected runoff components from different altitudes in baseline (1981–2010), near (2021–2050), and far future (2071–2100) periods

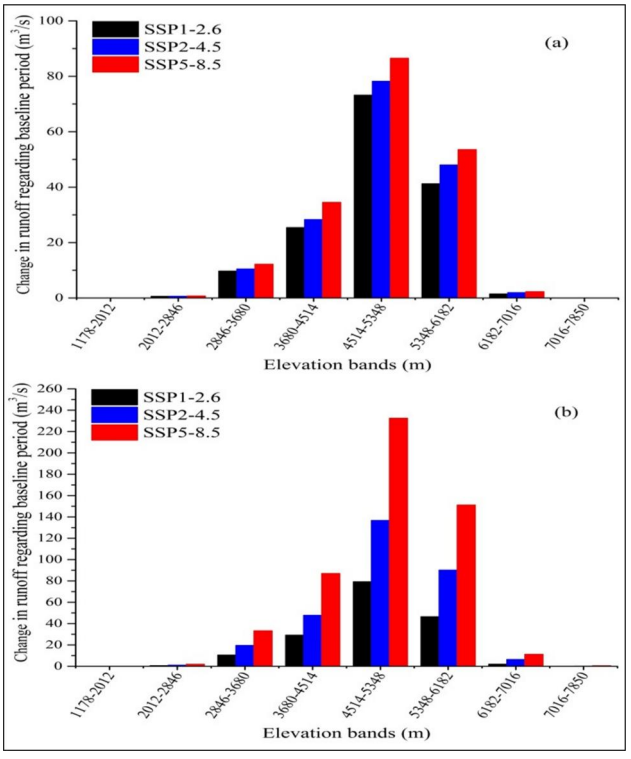

Figure 6. Projected change in the simulated runoff with reference to the baseline period from different altitudes of the Gilgit River basin in (a) the near future (2021–2050) and (b) the far future (2071–2100) under different SSPs.

is displayed in Figure 7(a–c). During the baseline period, the relative contribution of rainfall-runoff from the first elevation band (1178–2012) was found dominant while snowmelt contribution was minimal. From the second elevation band (2012–2846) to the fourth elevation band (3680–4514), the relative contribution of glacier melt was found dominant. The relative contribution of snowmelt gradually increases from the fourth elevation band (3680–4514) and it dominates the glacier melt in the fifth elevation band (4514–5348). The baseflow contribution starts from the fourth elevation band (3680–4514) and it becomes maximum in the fifth elevation band (4514–5348) as shown in Figure 7(a). Overall, it is detected a substantial amount of runoff contribution (i.e. nearly 76%) in the form of snowmelt, glacier melt, rainfall-runoff, and baseflow from elevations ranging from 3680 to 5348 m.

Similarly, in the near and far future, the relative contribution of rainfall-runoff is expected to be more dominant from the first elevation band (1178–2012) than other runoff components whereas from the second elevation band (2012–2846) to the fifth elevation band (4514–5348), the relative contribution of glacier melt runoff is expected to be dominant than other runoff components as shown in Figure 7(b,c). In comparison with the baseline period; the relative contribution of glacier melt is projected to gradually increase from the fourth elevation band (3680–4514) to the seventh elevation band (6182–7016) due to a significant rise in projected air temperature in the near and far future. Moreover, the small part of simulated runoff is also predicted to be contributed from the eighth elevation band (7016–7850) which depicts that the projected warming will badly impact the high altitude cryosphere i.e. above 6000 m elevation in the far future (Figure 7(c)).

3.6. Temporal variations in future projected simulated runoff components under different SSPs

The linear trend analysis of runoff components simulated by UBC WM in baseline, near, and far future under different SSPs are presented in Figure 8(a–g). During the baseline period (1981–2010), the simulated runoff of glacier melt is predicted to considerably increase at a rate of 1.26 cumec per annum followed by baseflow (0.38 cumec), and snowmelt (0.011 cumec) per annum while the rainfall-runoff is predicted to decrease with a change rate of −0.049 cumec per annum as shown in Figure 8(a).

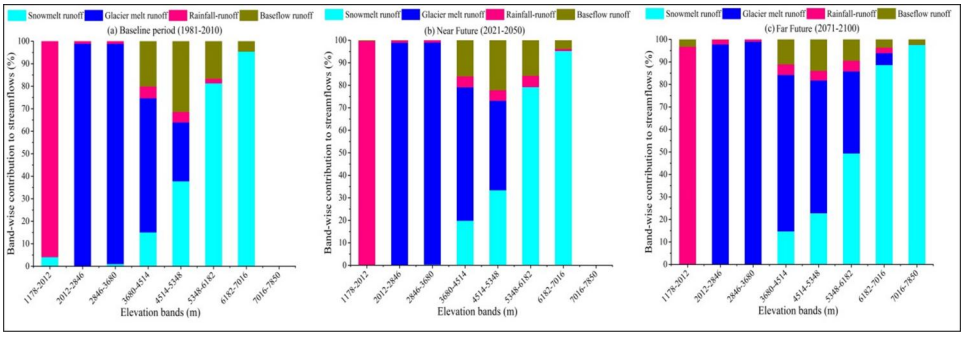

Figure 7. The relative contribution of future projected simulated runoff components of Gilgit River from different altitudes, in (a) baseline (1981–2010), (b) near future (2021–2050), and far future (2071–2100) under average SSPs.

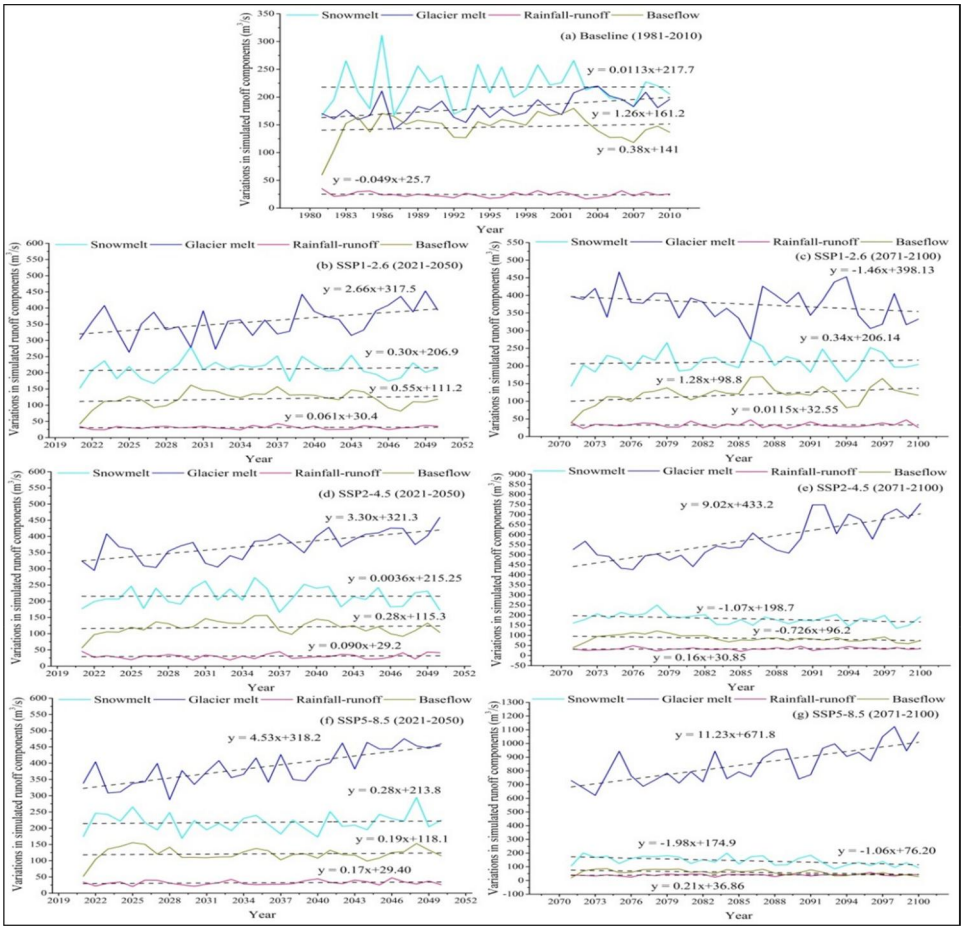

Figure 8. Temporal variations in future projected simulated runoff components in (a) baseline (1981–2010), (b, d, f) near future (2021–2050), and (c, e, g) far future (2071–2100) under different SSPs.

In the near future, the glacier melt runoff is expected to increase substantially followed by baseflow, snowmelt runoff, and rainfall runoff under all SSPs (Figure 8(b,d,f)). The glacier melt runoff is estimated to increase at a rate of 2.66, 3.30, and 4.53 cumec per annum under SSP1, SSP2, and SSP5, respectively. The snowmelt runoff is projected to increase at a rate of 0.30, 0.0036, and 0.28 cumec per annum under SSP1, SSP2, and SSP5, respectively. Similarly, the baseflow is projected to increase at a rate of 0.55, 0.28, and 0.19 cumec per annum under SSP1, SSP2, and SSP5, respectively in the near future. However, the rainfall-runoff is predicted to increase gradually at a rate of 0.061, 0.090, and 0.17 cumec per annum under SSP1, SSP2, and SSP5, respectively.

However, in the far future, the glacier melt runoff is predicted to decrease at a rate of −1.46 cumec per annum under SSP1 because of the projected decrease in air temperature under a low emission scenario (SSP1) as shown in Figure 8(c). Conversely, the baseflow, snowmelt, and rainfall-runoff are estimated to increase at a rate of 1.28, 0.34, and 0.012 cumec per annum under SSP1 due to a substantial increase in precipitation in the far future under SSP1. Besides, the glacier melt runoff is predicted to significantly increase at a rate of 9.02 and 11.23 cumec per annum whereas, the

snowmelt and baseflow are estimated to decrease under SSP2 and SSP5, respectively. However, a gradual increase in rainfall-runoff is predicted in the far future under all SSPs (Figure 8(c,e,g)). Overall, it is observed that baseflow is largely dependent on snowmelt runoff.

4. Discussions

In previous hydrological studies of this region such as (Adnan et al. 2017; Garee et al. 2017; Ali et al. 2018; Hayat et al. 2019; Dolk et al. 2020; Fatima et al. 2020; Latif et al. 2020; Nazeer et al. 2022); the estimation of spatiotemporal variations in sources of runoff and their relative contribution to total river runoff were neglected. The current study is unique because this will determine the spatiotemporal variations in sources of runoff and their relative contributions to the streamflows of the Gilgit River under the latest SSPs. The main outcomes obtained from the current study are discussed below:

On average, the linear trend analysis of time series data revealed a substantial increase in the magnitude of mean annual temperature during baseline (0.83 °C); near future (0.87, 1.09, and 1.70 °C), and far future (−0.33, 0.77, and 2.10 °C) per period under SSP1, SSP2 and SSP5, respectively. Similarly, a study conducted by Lutz et al. (2019) projected an increase in temperature magnitude by 2.1 and 2.7 °C in a 1.5 and 2 °C warmer world, respectively, in the HKH region. Likewise, a study conducted by Latif et al. (2020) also projected an increase in the mean annual temperature of the Gilgit catchment between 0.7 and 2.6 °C during 2039–2070. Moreover, it has been projected more warming rate in the near future than far future under low and medium emission scenarios. Similar results were obtained by a study conducted by Ali et al. (2015), they also observed a slow increase in air temperature towards the end of the twenty first century (2071–2100) as compared to the near future (2041–2071) in UIB under medium emission scenario. Besides, it is projected warming to a greater extent at high-altitude stations of the Gilgit River basin (i.e. Ziarat and Khunjerab) than low altitude stations (i.e. Gilgit and Gupis) in the near and far future under all SSPs. Similarly, the studies performed by Li et al. (2020) and Mountain Research Initiative EDW Working Group (2015) also observed that the rate of warming is intensified by elevation and global warming is being experienced more rapidly at high elevations than at low elevations. The future projected scenarios also exhibited an increasing trend in annual precipitation magnitude with respect to baseline in the near and far future. Regarding the baseline period, the mean annual precipitation is projected to increase by 6.4%, 5.85%, and 8.0% under SSP1, SSP2, and SSP5, respectively in the near future while it is projected to increase by 8.45%, 6.2%, and 12.9% in far future under SSP1, SSP2 and SSP5, respectively. Similarly, the outcomes of future precipitation projections performed by Nazeer et al. (2022) indicated a 12–32% increase in precipitation during the twenty first century in the Hunza River basin. However, a study conducted by Shah et al. (2020) also projected an increase in annual average precipitation of UIB ranging from 2.4% to 2.5% (during mid) and 6.0% to 4.6% (during the end) of the twenty first century under RCP4.5 and 8.5, respectively.

Moreover, due to an increase in air temperature and precipitation, the simulated runoff of the Gilgit River is also projected to increase by 27%, 30%, and 33% per period under SSP1, SSP2, and SSP5, respectively whereas in the far future, it is expected to increase by 30%, 53% and 91% per period under SSP1, SSP2 and SSP5, respectively regarding baseline period.

Likewise, a study conducted by Ul Hasson et al. (2019) projected an increase of 34 and 43% in the streamflows of the UIB in a 1.5 and 2 °C warmer world, respectively. Likewise, Hayat et al. (2019) projected a 14 to 90% increase in the mean annual discharge of Hunza River under all RCPs during the mid to late-twenty first century. However, Adnan et al. (2017) estimated a 67% increase in the mean annual discharge of the Gilgit River due to an increase of 3 °C under RCP4.5 by the end of the twenty first century. Similarly, with reference to the baseline period, the simulated runoff in the near and far future is projected to increase more in summer (JJA) followed by spring (MAM) and autumn (SON) seasons from low to high emission scenarios whereas it is projected a decrease in winter (DJF) runoff under all SSPs. Similarly, a study conducted by Latif et al. (2020) estimated a 5.6 to 19.8% increase in summer flows of the Gilgit River due to a rise in mean annual temperature between 0.7 and 2.6 °C during 2039–2070.

Moreover, out of eight elevation bands of the Gilgit River basin; the simulated runoff is projected to substantially increase from the fifth elevation band (4514–5348) followed by the sixth (5348–6182), fourth (3680–4514) and third (2846–3680) elevation band with reference to baseline period based on glacier cover area in the respective elevation bands in the near and far future under all SSPs. This is because of enhanced glaciers melting as a result of a significant increase in high-altitude air temperature than to low altitude in the Gilgit River basin as projected under SSPs and this has been confirmed in previous studies (i.e. Mountain Research Initiative EDW Working Group 2015; Li et al. 2020) that the rate of warming is increased by elevation and high altitudes areas are affected more rapidly by global warming as compared to low altitude areas in HMA and Tibetan Plateau.

The relative contribution of rainfall-runoff is projected to be dominant from the first elevation band (1178–2012) in baseline, near, and far future periods. The glacier melt runoff is projected to be dominant from the second elevation band (2012–2846) to the fourth elevation band (3680–4514) in the baseline period and the second to fifth elevation band (4514–5348) in the near and far future. However, the simulated runoff in the form of glacier melt is projected to significantly increase from the fifth (4514–5348) to the seventh elevation band (6182–7016) in the far future because of a significant increase in projected air temperature at high altitude meteorological stations of the Gilgit River basin. The outcomes of our study are supported by the study conducted by Kraaijenbrink et al. (2017), they also projected a substantial loss in the present-day ice mass of HMA by 2100 at a rate of 26, 49, 51 and 64% per period under RCP2.6, 4.5, 6.0 and 8.5, respectively. Similarly, a few other studies conducted by i.e. (Kraaijenbrink et al. 2017; Bolch et al. 2019; Hock et al. 2019; Rounce et al. 2020) also projected the shrinking of HMA glaciers ranging from 40 to 70% under different RCPs. Moreover, in the far future, the eighth elevation band (7016–7850) is also projected to contribute part of simulated runoff in the form of snowmelt and baseflow which illustrates that projected warming will badly impact the high altitude cryosphere i.e. above 6000 m elevation.

5. Conclusions

The untimely start of melting snow/glaciers causes an alteration in the magnitude of runoff and ultimate water availability earlier in the year at the seasonal scale. It has been detected a change in the hydrology, cryosphere, and climate of the HKH region in recent decades, and this warming is expected to persist throughout the twenty first century. Keeping in view the above situation, the current study is designed to project

spatiotemporal variations in runoff and sources of runoff simulated by UBC WM and their relative contributions to total runoff under low, medium, and high emission scenarios in the near and far future periods. The main outcomes of this study are given below:

1. The future projected maximum, minimum, and average temperature is projected to increase more in the near future than far future under low and medium emission scenarios, whereas the case is reversed in the far future where it is estimated a substantial increase in the magnitude of air temperature under high emission scenario. Moreover, a substantial warming rate is projected at high altitudes stations of the Gilgit River basin than low altitudes in the near and far future under all SSPs. Similarly, the trend analysis exhibited a greater increase in the magnitude of annual precipitation in the near future as compared to the far future under all SSPs.
2. Moreover, with reference to the baseline period, the runoff simulated by UBC WM is expected to increase at a rate of 27%, 30%, and 33% in the near future while 30%, 53%, and 91% per period in far future under SSP1, SSP2 and SSP5, respectively. Similarly, with respect to the baseline period, the summer (JJA) runoff is projected to increase substantially followed by spring (MAM) and autumn (SON) seasons while a decrease in winter (DJF) runoff is projected in the near and far future under all SSPs.
3. The fifth elevation band (4514–5348) being the most glaciated is projected to contribute maximum runoff followed by the sixth (5348–6182), fourth (3680–4514), and third (2846–3680) elevation bands because of an increase in projected warming at high altitudes in the near and far future under all SSPs.
4. All sources of runoff of the Gilgit River are projected to significantly increase in the near future with glacier melt runoff as the dominant source of runoff under all SSPs while it has been predicted a substantial increase in the glacier melt runoff and a decrease in snowmelt and baseflow is projected due to decrease in winter (DJF) precipitation under SSP2 and SSP5 in the far future.

Acknowledgments

The authors are grateful to the Pakistan Meteorological Department (PMD) and Surface Water Hydrology Project of the Water and Power Development Authority (SWHP-WAPDA) for providing the required hydro-meteorological data to conduct this study.

Disclosure statement

The authors have no conflict of interest to declare.

Funding

Financial support for this research was provided by the National Natural Science Foundation of China (Grant no. 42171129), the Second Tibetan Plateau Scientific Expedition and Research Program (STEP, Grant no. 2019QZKK0208), the International Science and Technology and Innovation Cooperation Program of the State Key Research and Development Program (Grant

no. 2021YFE0116800). This research is also supported by Pakistan Science Foundation (grant no. PSF/CRP/Consrm-488) and (grant no. SGP-WWF-5090103).

Data availability statement

The hydro-meteorological data used in the current study is confidential and cannot be shared with a third party; however, it can be directly acquired from the Pakistan Meteorological Department and Surface Water Hydrology Project of Water and Power Development Authority, Pakistan through proper channels. However, the model datasets generated for this study are available on request to the corresponding author.

References

Adnan M, Liu S, Saifullah M, Iqbal M, Ali AF, Mukhtar MA. 2022. Spatiotemporal variations in runoff and runoff components in response to climate change in a glacierized subbasin of the Upper Indus Basin, Pakistan. Front Earth Sci. 10:970349. doi: 10.3389/feart.2022.970349.

Adnan M, Nabi G, Kang S, Zhang G, Adnan RM, Anjum MN, Iqbal M, Ali AF. 2017. Snowmelt runoff modelling under projected climate change patterns in the Gilgit River basin of Northern Pakistan. Pol J Environ Stud. 26(2):525–542. doi: 10.15244/pjoes/66719.

Ali AF, Xiao C-d, Zhang X-p, Adnan M, Iqbal M, Khan G. 2018. Projection of future stream-flow of the Hunza River Basin, Karakoram Range (Pakistan) using HBV hydrological model. J Mt Sci. 15(10):2218–2235. doi: 10.1007/s11629-018-4907-4.

Ali S, Li D, Congbin F, Khan F. 2015. Twenty-first century climatic and hydrological changes over Upper Indus Basin of Himalayan region of Pakistan. Environ Res Lett. 10(1):014007. doi: 10.1088/1748-9326/10/1/014007.

Bolch T, Shea JM, Liu S, Azam FM, Gao Y, Gruber S, Immerzeel WW, Kulkarni A, Li H, Tahir AA. 2019. Status and change of the cryosphere in the extended Hindu Kush Himalaya region. In: Wester P, Mishra A, Mukherji A, Shrestha A, editors. The Hindu Kush Himalaya assessment: mountains, climate change, sustainability and people. Cham, Switzerland: Springer; p. 209–255. doi: 10.1007/978-3-319-92288-1_7.

Cheng WY, Steenburgh WJ. 2007. Strengths and weaknesses of MOS, running-mean bias removal, and Kalman filter techniques for improving model forecasts over the western United States. Weather Forecast. 22(6):1304–1318. doi: 10.1175/2007WAF2006084.1.

Dahri ZH, Ludwig F, Moors E, Ahmad S, Ahmad B, Ahmad S, Riaz M, Kabat P. 2021. Climate change and hydrological regime of the high-altitude Indus basin under extreme climate scenarios. Sci Total Environ. 768:144467. doi: 10.1016/j.scitotenv.2020.144467.

Dolk M, Penton DJ, Ahmad MD. 2020. Amplification of hydrological model uncertainties in projected climate simulations of the Upper Indus Basin: does it matter where the water is coming from? Hydrol Processes. 34(10):2200–2218. doi: 10.1002/hyp.13718.

Fatima E, Hassan M, Hasson S, Ahmad B, Ali SSF. 2020. Future water availability from the western Karakoram under representative concentration pathways as simulated by CORDEX South Asia. Theor Appl Climatol. 141(3-4):1093–1108. doi: 10.1007/s00704-020-03261-w.

Gao Y, Liu S, Qi M, Xie F, Wu K, Zhu Y. 2021. Glacier-related hazards along the International Karakoram Highway: status and future perspectives. Front Earth Sci. 9:611501. doi: 10.3389/feart.2021.611501.

Garee K, Chen X, Bao A, Wang Y, Meng F. 2017. Hydrological modeling of the upper Indus basin: a case study from a high-altitude glacierized catchment Hunza. Water. 9(1):17. doi: 10.3390/w9010017.

Hasson S, Böhner J, Lucarini V. 2017. Prevailing climatic trends and runoff response from Hindukush–Karakoram–Himalaya, upper Indus Basin. Earth Syst Dynam. 8(2):337–355. doi: 10.5194/esd-8-337-2017.

Hayat H, Akbar TA, Tahir AA, Hassan QK, Dewan A, Irshad M. 2019. Simulating current and future river flows in the Karakoram and Himalayan regions of Pakistan using snowmelt-runoff model and RCP scenarios. Water. 11(4):761. doi: 10.3390/w11040761.

Hewitt K. 2011. Glacier change, concentration, and elevation effects in the Karakoram Himalaya, Upper Indus Basin. Mt Res Dev. 31(3):188–200. doi: 10.1659/MRD-JOURNAL-D-11-00020.1.

Hock R, Rasul G, Adler C, Cáceres B, Gruber S, Hirabayashi Y, Jackson M, Kääb A, Kang S, Kutuzov S. 2019. High mountain areas. In: Pörtner H-O, Roberts DC, Masson-Delmotte V, et al. editors. Special report on the ocean and cryosphere in a changing climate. New York, USA: IPCC; pp. 131–202.

Hussain D, Kuo C-Y, Hameed A, Tseng K-H, Jan B, Abbas N, Kao H-C, Lan W-H, Imani M. 2019. Spaceborne satellite for snow cover and hydrological characteristics of the Gilgit river basin, Hindukush–Karakoram mountains, Pakistan. Sensors. 19(3):531. doi: 10.3390/s19030531.

Jaagus J. 2006. Climatic changes in Estonia during the second half of the 20th century in relationship with changes in large-scale atmospheric circulation. Theor Appl Climatol. 83(1-4): 77–88. doi: 10.1007/s00704-005-0161-0.

Kendall MG. 1975. Rank correlation methods. 4th ed. London (UK): Charles Griffin.

Kraaijenbrink PD, Bierkens MF, Lutz AF, Immerzeel W. 2017. Impact of a global temperature rise of 1.5 degrees Celsius on Asia's glaciers. Nature. 549(7671):257–260. doi: 10.1038/nature23878.

Krishnan R, Shrestha AB, Ren G, Rajbhandari R, Saeed S, Sanjay J, Syed MA, Vellore R, Xu Y, You Q. 2019. Unravelling climate change in the Hindu Kush Himalaya: rapid warming in the mountains and increasing extremes. In: Wester P, Mishra A, Mukherji A, Shrestha A. editors. The Hindu Kush Himalaya assessment: mountains, climate change, sustainability and people. Cham, Switzerland: Springer; p. 57–97. doi: 10.1007/978-3-319-92288-1_3

Lanzante JR. 1996. Resistant, robust and non-parametric techniques for the analysis of climate data: theory and examples, including applications to historical radiosonde station data. Int J Climatol. 16(11):1197–1226. doi: 10.1002/(SICI)1097-0088(199611)16:11<1197::AID-JOC89>3.0.CO;2-L.

Latif Y, Ma Y, Ma W, Muhammad S, Adnan M, Yaseen M, Fealy R. 2020. Differentiating snow and glacier melt contribution to runoff in the Gilgit River basin via degree-day modelling approach. Atmosphere. 11(10):1023. doi: 10.3390/atmos11101023.

Li B, Chen Y, Shi X. 2020. Does elevation-dependent warming exist in high mountain Asia? Environ Res Lett. 15(2):024012. doi: 10.1088/1748-9326/ab6d7f.

Loukas A, Vasiliades L. 2014. Streamflow simulation methods for ungauged and poorly gauged watersheds. Nat Hazards Earth Syst Sci. 14(7):1641–1661. doi: 10.5194/nhess-14-1641-2014.

Lutz AF, ter Maat HW, Wijngaard RR, Biemans H, Syed A, Shrestha AB, Wester P, Immerzeel WW. 2019. South Asian river basins in a 1.5 C warmer world. Reg Environ Change. 19(3): 833–847. doi: 10.1007/s10113-018-1433-4.

Mann HB. 1945. Non-parametric tests against trend. Econometrica. 13(3):245. doi: 10.2307/1907187.

Mountain Research Initiative EDW Working Group. 2015. Elevation-dependent warming in mountain regions of the world. Nat Clim Change. 5(5):424–430.

Nash JE, Sutcliffe JV. 1970. River flow forecasting through conceptual models part I – a discussion of principles. J Hydrol. 10(3):282–290. doi: 10.1016/0022-1694(70)90255-6.

Nazeer A, Maskey S, Skaugen T, McClain ME. 2022. Changes in the hydro-climatic regime of the Hunza Basin in the Upper Indus under CMIP6 climate change projections. Sci Rep. 12(1):21442. doi: 10.1038/s41598-022-25673-6.

Ougahi JH, Cutler ME, Cook SJ. 2022. Assessing the Karakoram Anomaly from long-term trends in earth observation and climate data. Remote Sens Appl Soc Environ. 28:100852. doi: 10.1016/j.rsase.2022.100852.

Quick M C, Pipes A. 1977. U.B.C. WATERSHED MODEL / Le modèle du bassin versant U.C.B. Hydrol Sci Bull 22(1):153–161. doi: 10.1080/02626667709491701.

Quick M, Pipes A. 1972. Daily and seasonal runoff forecasting with a water budget model. In: The role of snow and ice in hydrology. Proceedings of the UNESCO/WMO/IAHS Symposium; Sep; Banff. IAHS.

Rounce DR, Hock R, Shean DE. 2020. Glacier mass change in High Mountain Asia through 2100 using the open-source python glacier evolution model (PyGEM). Front Earth Sci. 7: 331. doi: 10.3389/feart.2019.00331.

Saifullah M, Liu S, Adnan M, Ashraf M, Zaman M, Hashim S, Muhammad S. 2020. Risks of glaciers lakes outburst flood along China Pakistan economic corridor. In: Kanao M, Godone D, Dematteis N, editor. Glaciers and the polar environment. London, UK: IntechOpen. doi: 10.5772/intechopen.93459.

Sen PK. 1968. Estimates of the regression coefficient based on Kendall's tau. J Am Stat Assoc. 63(324):1379–1389. doi: 10.1080/01621459.1968.10480934.

Shah MI, Khan A, Akbar TA, Hassan QK, Khan AJ, Dewan A. 2020. Predicting hydrologic responses to climate changes in highly glacierized and mountainous region Upper Indus Basin. R Soc Open Sci. 7(8):191957. doi: 10.1098/rsos.191957.

Snowmelt runoff simulation during early 21st century using hydrological modelling in the Snow-Fed Terrain of Gilgit River Basin (Pakistan). 2019. Advances in Sustainable and Environmental Hydrology, Hydrogeology, Hydrochemistry and Water Resources: proceedings of the 1st Springer Conference of the Arabian Journal of Geosciences (CAJG-1), Tunisia 2018; Springer.

Soncini A, Bocchiola D, Confortola G, Bianchi A, Rosso R, Mayer C, Lambrecht A, Palazzi E, Smiraglia C, Diolaiuti G. 2015. Future hydrological regimes in the Upper Indus basin: a case study from a high-altitude glacierized catchment. J Hydrometeorol. 16(1):306–326. doi: 10.1175/JHM-D-14-0043.1.

Sperna Weiland F, Van Beek L, Kwadijk J, Bierkens M. 2010. The ability of a GCM-forced hydrological model to reproduce global discharge variability. Hydrol Earth Syst Sci. 14(8): 1595–1621. doi: 10.5194/hess-14-1595-2010.

Su F, Pritchard HD, Yao T, Huang J, Ou T, Meng F, Sun H, Li Y, Xu B, Zhu M, et al. 2022. Contrasting fate of western Third Pole's water resources under 21st century climate change. Earth's Future. 10(9):e2022EF002776. doi: 10.1029/2022EF002776.

Tahir AA, Chevallier P, Arnaud Y, Neppel L, Ahmad B. 2011. Modeling snowmelt-runoff under climate scenarios in the Hunza River basin, Karakoram Range, Northern Pakistan. J Hydrol. 409(1-2):104–117. doi: 10.1016/j.jhydrol.2011.08.035.

Ul Hasson S, Saeed F, Böhner J, Schleussner C-F. 2019. Water availability in Pakistan from Hindukush–Karakoram–Himalayan watersheds at 1.5° C and 2° C Paris Agreement targets. Adv Water Resour. 131:103365. doi: 10.1016/j.advwatres.2019.06.010.

Ul Hussan W, Khurram Shahzad M, Seidel F, Costa A, Nestmann F. 2020. Comparative assessment of spatial variability and trends of flows and sediments under the impact of climate change in the Upper Indus Basin. Water. 12(3):730. doi: 10.3390/w12030730.

Wijngaard RR, Biemans H, Lutz AF, Shrestha AB, Wester P, Immerzeel WW. 2018. Climate change vs. socio-economic development: understanding the future South Asian water gap. Hydrol Earth Syst Sci. 22(12):6297–6321. doi: 10.5194/hess-22-6297-2018.

Wijngaard RR, Lutz AF, Nepal S, Khanal S, Pradhananga S, Shrestha AB, Immerzeel WW. 2017. Future changes in hydro-climatic extremes in the Upper Indus, Ganges, and Brahmaputra River basins. PLoS One. 12(12):e0190224. doi: 10.1371/journal.pone.0190224.

Yu W, Yang Y-C, Savitsky A, Alford D, Brown C, Wescoat J, Debowicz D, Robinson S. 2013. Hydrology and glaciers in the Upper Indus Basin: Impacts of Climate Risks on Water and Agriculture. 57–76. © International Bank for Reconstruction and Development/The World Bank. Washington, DC. http://hdl.handle.net/10986/13834.

Zhang X-C. 2005. Spatial downscaling of global climate model output for site-specific assessment of crop production and soil erosion. Agric for Meteorol. 135(1-4):215–229. doi: 10.1016/j.agrformet.2005.11.016.

Appendix

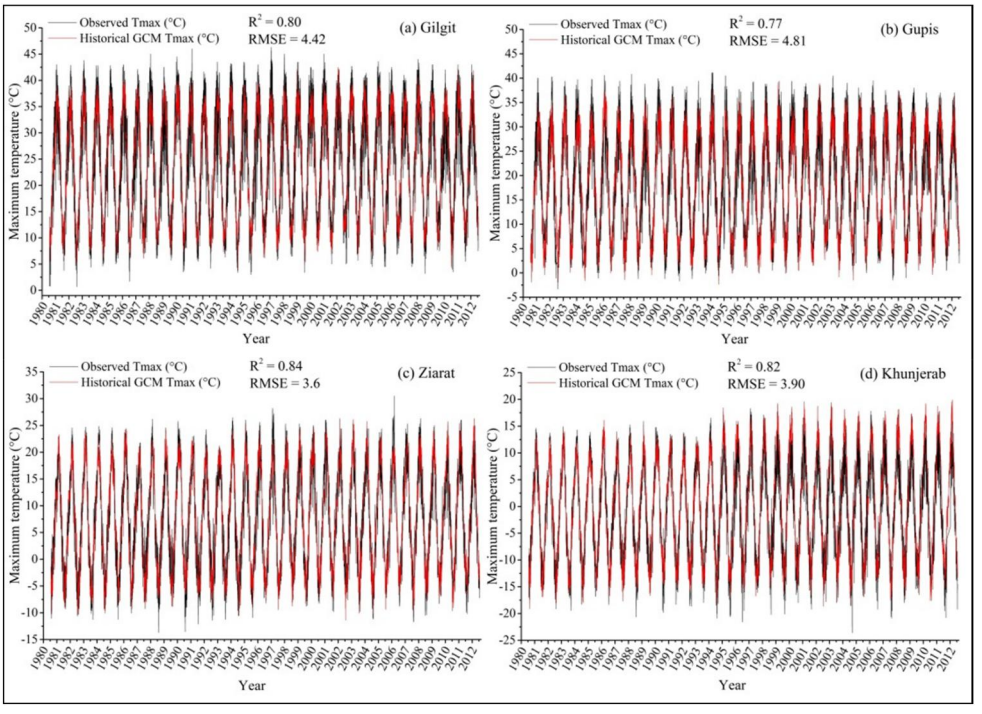

Figure A1. Comparisons of observed maximum temperature of four meteorological satiations of the Gilgit River basin with the ensemble mean GCM historical data for the period of 1981–2012.

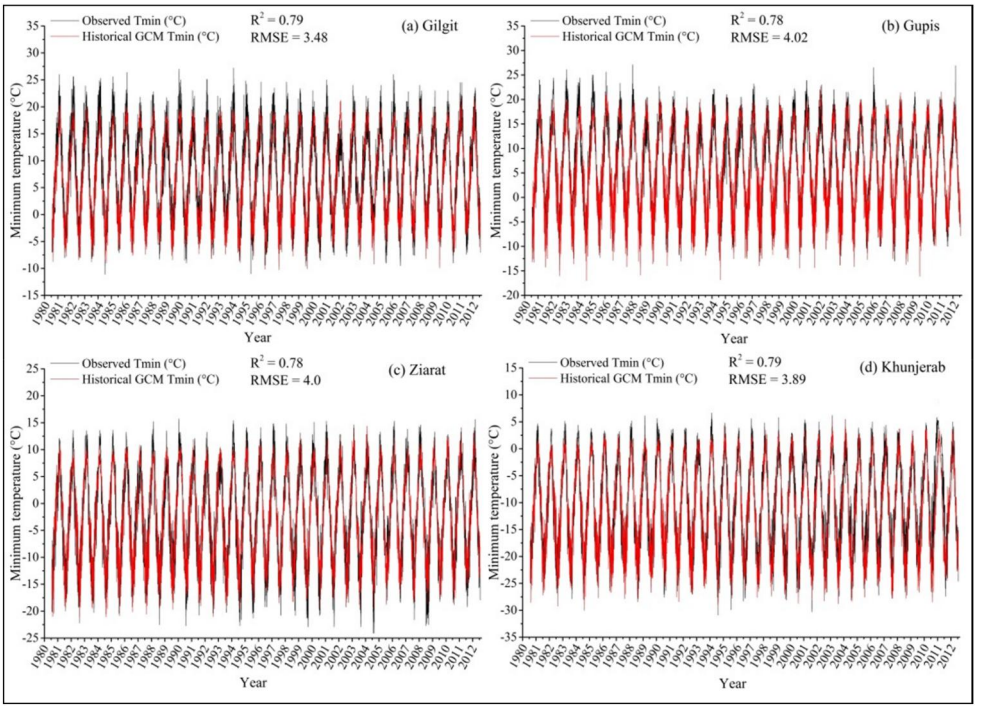

Figure A2. Comparisons of observed minimum temperature of four meteorological satiations of the Gilgit River basin with the ensemble mean GCM historical data for the period of 1981–2012.

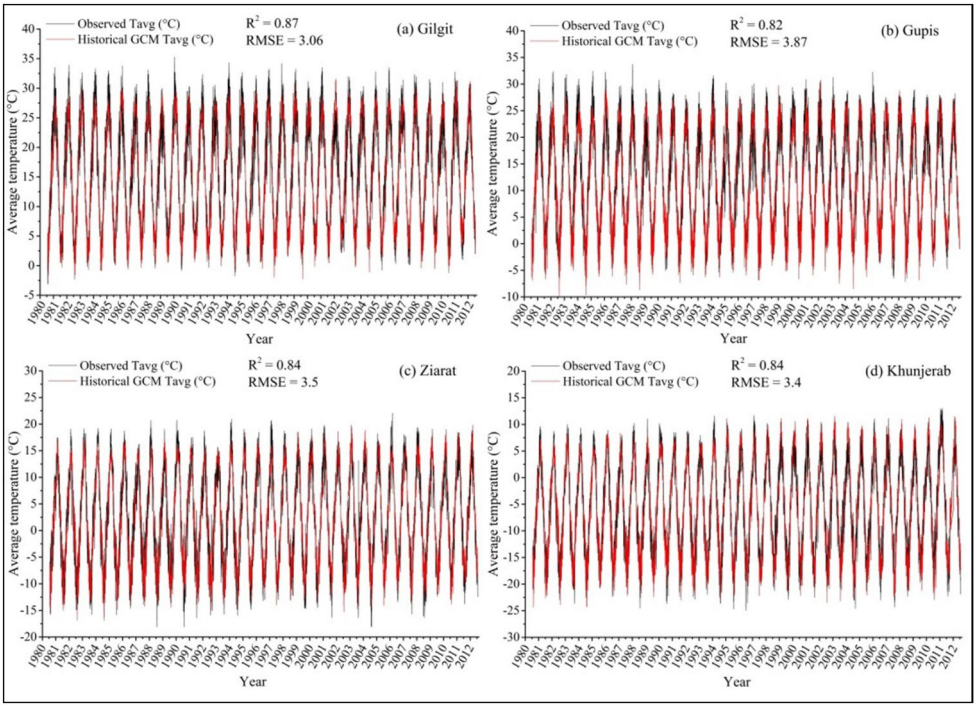

Figure A3. Comparisons of observed average temperature of four meteorological satiations of the Gilgit River basin with the ensemble mean GCM historical data for the period of 1981–2012.

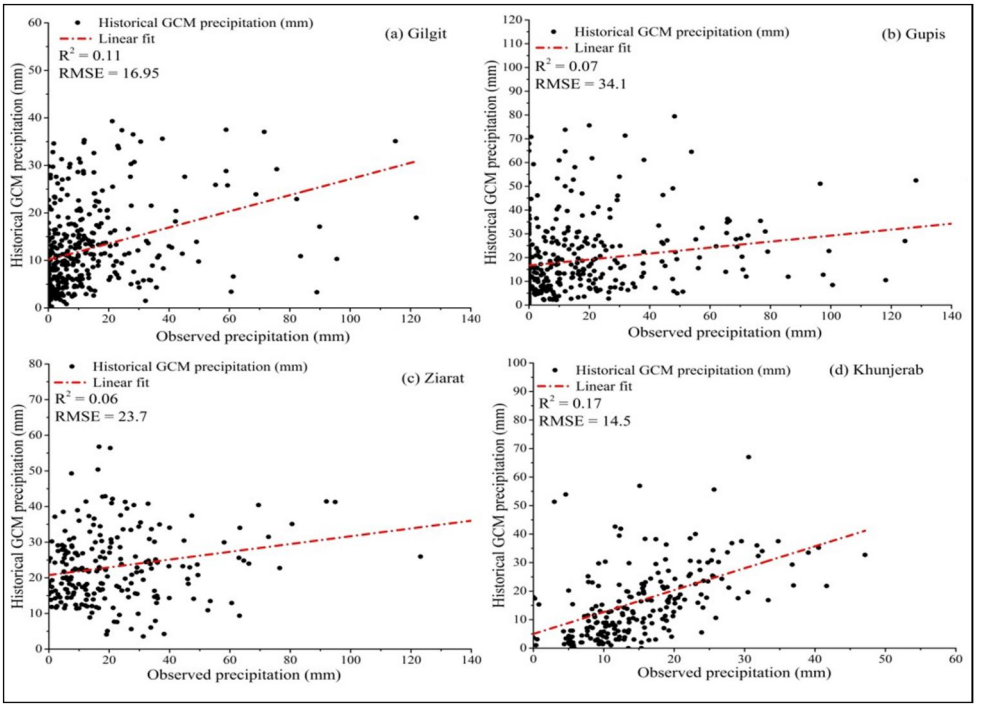

Figure A4. Comparisons of observed precipitation of four meteorological satiations of the Gilgit River basin with the ensemble mean GCM historical data for the period of 1981–2012 at monthly time scale.

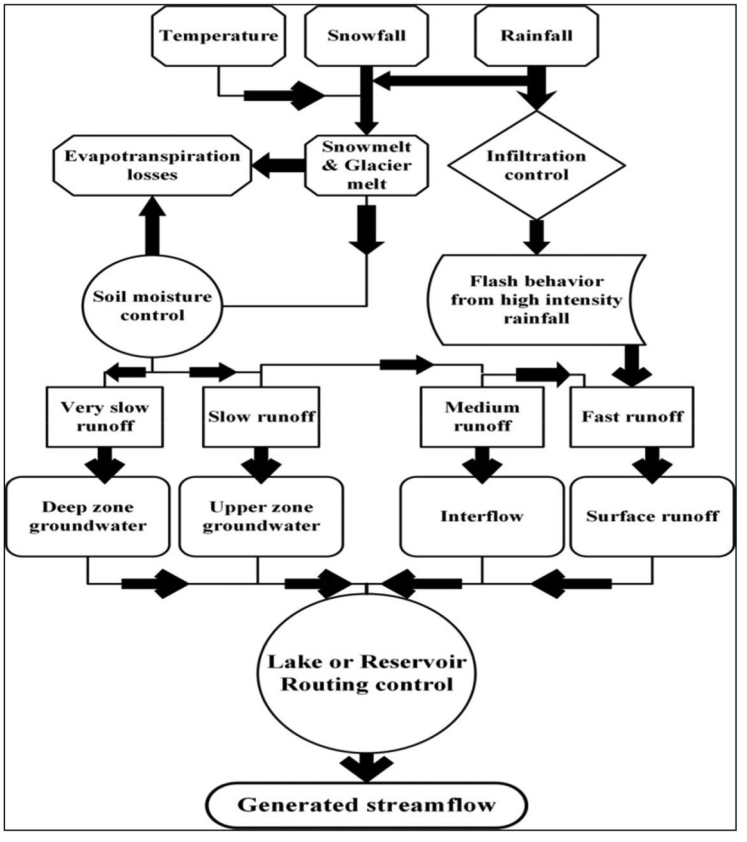

Figure A5. Process flow diagram of the UBC WM.

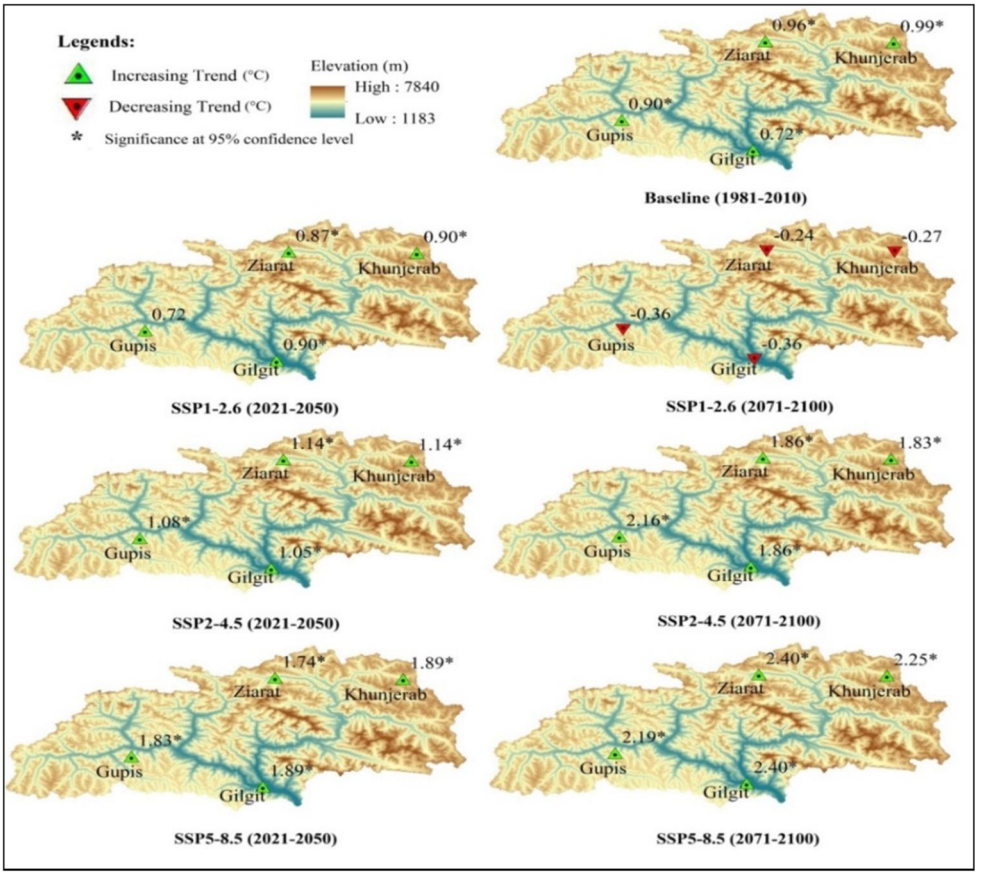

Figure A6. Change in the magnitude of future projected maximum temperature under different SSPs in baseline (1981–2010), near future (2021–2050), and far future (2071–2100).

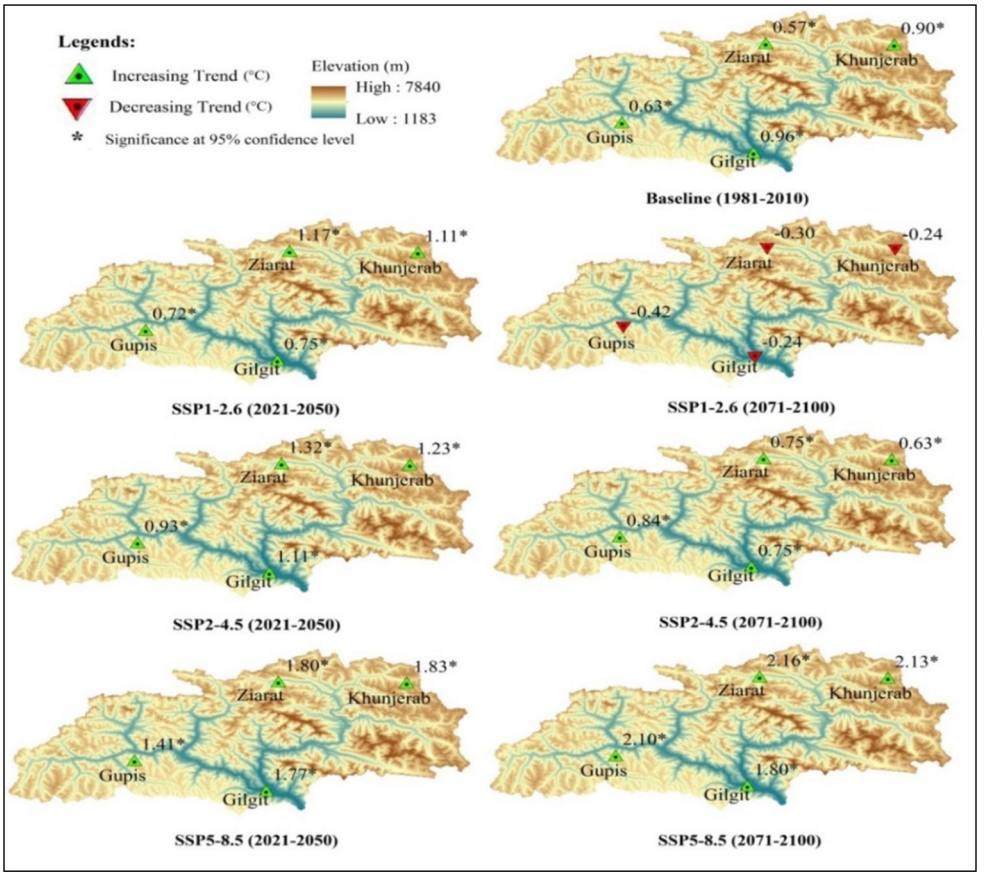

Figure A7. Change in the magnitude of future projected minimum temperature under different SSPs in baseline (1981–2010), near future (2021–2050), and far future (2071–2100).

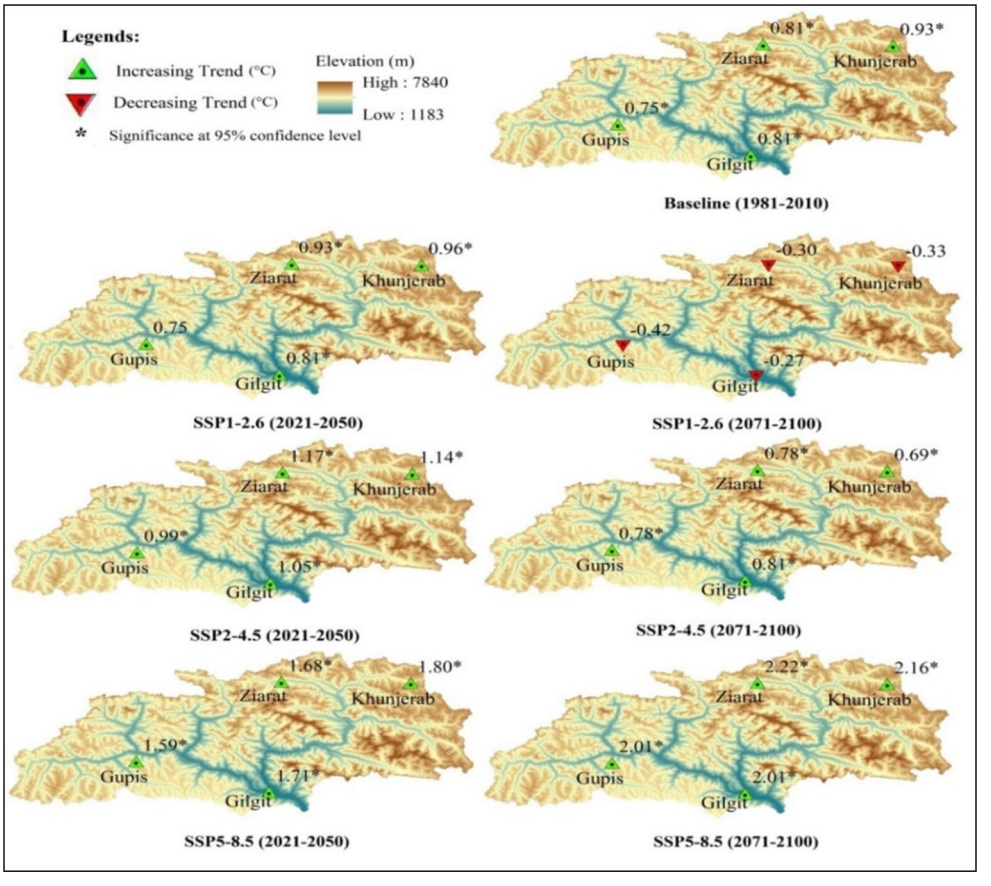

Figure A8. Change in the magnitude of future projected average temperature under different SSPs in baseline (1981–2010), near future (2021–2050), and far future (2071–2100).

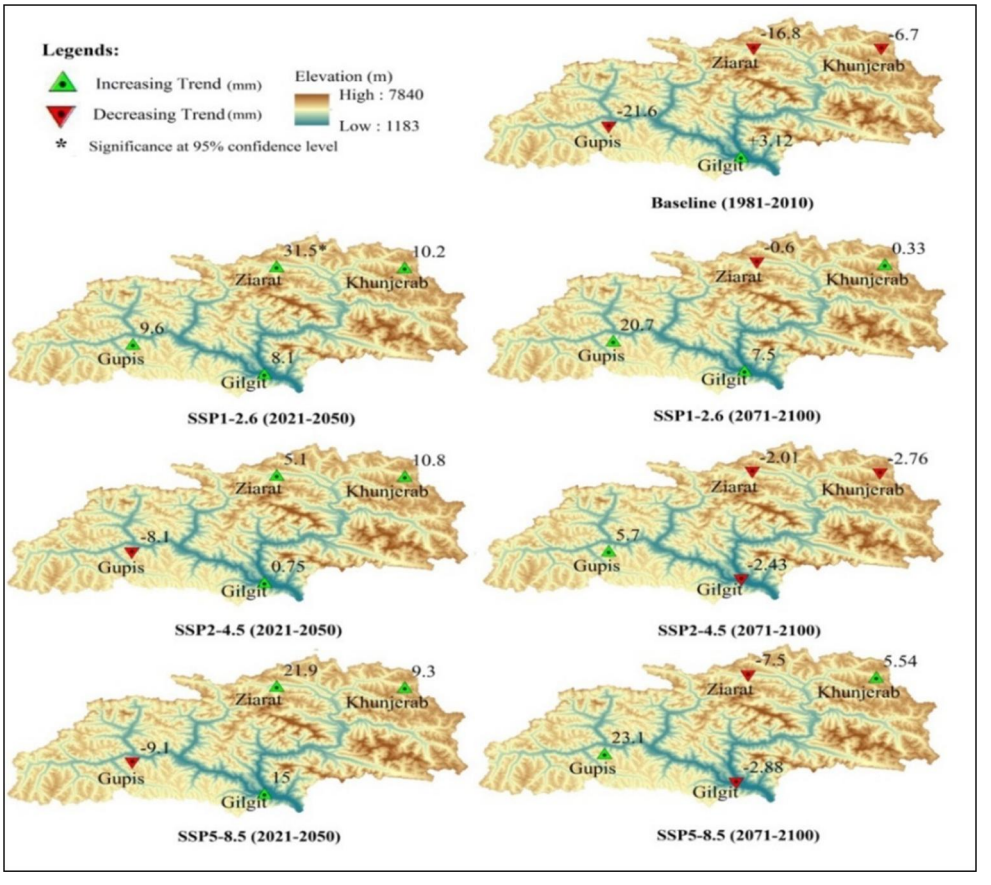

Figure A9. Change in the magnitude of future projected annual precipitation under different SSPs in the baseline (1981–2010), near future (2021–2050), and far future (2071–2100).

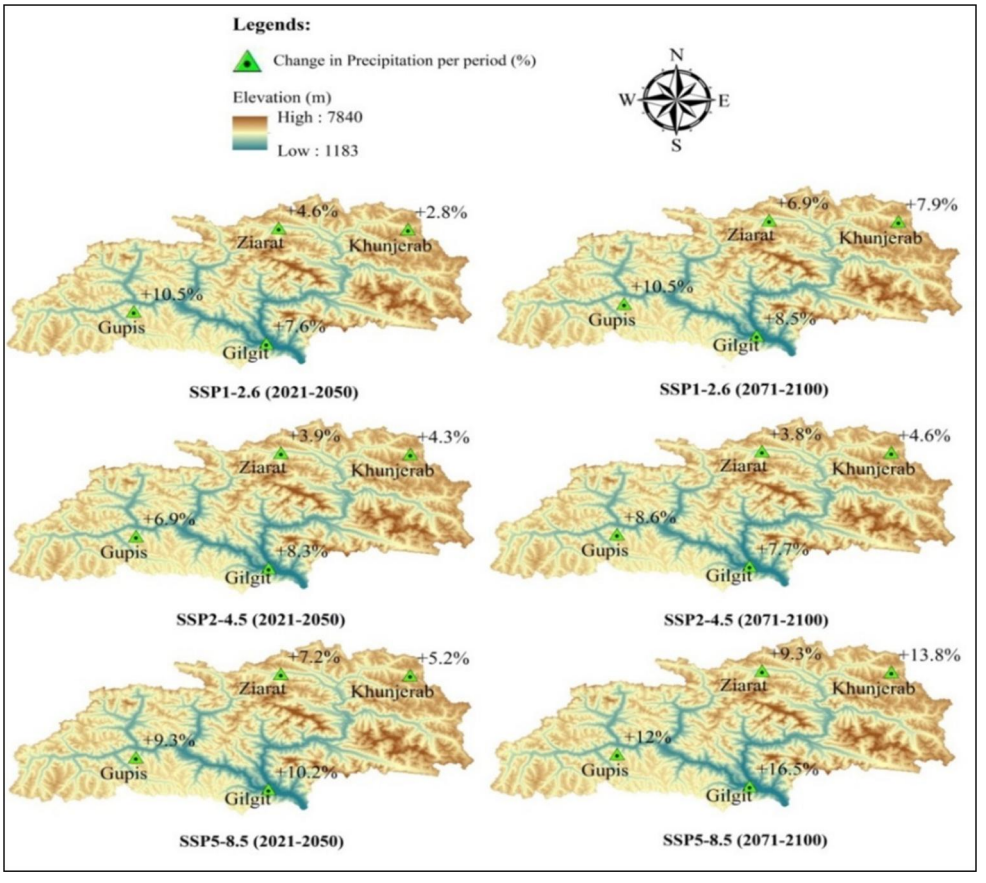

Figure A10. Percentage change in future projected annual precipitation regarding baseline period in the near (2021–2050) and far future (2071–2100) under different SSPs.